Journal of Catalysis 438 (2024) 115696

Contents lists available at ScienceDirect

Journal of Catalysis

journal homepage: www.elsevier.com/locate/jcat

Research article

The Rôle of Iron in Zeolite Beta for deNOx Catalysis

Jamal Abdul Nasir [a], Jingcheng Guan [a], Thomas W. Keal [d], You Lu [d], Alexey A. Sokol [a], C. Richard A. Catlow [a,b,c,*]

[a] Department of Chemistry, Kathleen Lonsdale Materials Chemistry University College London, 20 Gordon Street, London WC1H 0AJ, United Kingdom
[b] UK Catalysis Hub, Research Complex at Harwell, Rutherford Appleton Laboratory, R92 Harwell, Oxfordshire OX11 0FA, United Kingdom
[c] School of Chemistry, Cardiff University, Park Place, Cardiff CF10 3AT, United Kingdom
[d] STFC Daresbury Laboratory, Scientific Computing Department, Keckwick Lane, Warrington WA4 4AD, United Kingdom

ARTICLE INFO

Keywords:
Fe-Zeolite
deNOx Catalysis
Hybrid QM/MM
NH_3-SCR
Reaction Mechanism

ABSTRACT

Selective catalytic reduction with ammonia (NH_3-SCR) is a widely used deNOx process, employing zeolitic catalysts. Here, we examine framework substituted and extra-framework exchanged transition metal zeolite catalysts, in the extensively studied Fe – zeolite Beta focusing on the influence of the transition metal cation on the NH_3-SCR reaction, and aiming to unravel the underlying mechanisms and their impact on catalytic performance. We use hybrid multiscale density functional theory (DFT)/molecular mechanics to investigate the NH_3-SCR at various Fe-BEA active sites including systems with both framework and extra-framework Fe cations. The catalytically active sites under investigation include Fe-Fe_F-BEA, Fe-Al_F-BEA, and Cu-Fe_F-BEA, (where the subscript F indicates framework species) on which the formation and consumption of key intermediates of both oxidation and reduction half cycles species are analysed. We show the distinctive ability of framework Fe sites to promote the formation of key nitrate and nitrosamine intermediates. Furthermore, we find a strong binding affinity of NH_3 with framework Fe systems including Cu(II)-Fe_F-BEA, Fe(III)-Fe_F-BEA, and H-Fe_F-BEA compared to framework Al systems (Fe(III)-Al_F-BEA). We explore the reduction potential of the framework Fe^{3+}/Fe^{2+} in BEA zeolite and establish its feasibility in the presence of a Brønsted acid site. Our calculations clearly predict the bimetallic Cu-Fe_F system to be the best catalyst which supports a recent experimental report by Yue *et al.* (Chem. Eng. J. 2020, 398, 125515) for a related FeCu-SSZ-13 (CHA) zeolite. We provide a new understanding of the reactivity of Fe-BEA zeolites, suggesting the advantages of framework Fe over Al sites in NH_3-SCR reactions, and establishing a foundation for interpretation of the rôle of framework cations in metal-exchanged zeolites.

1. Introduction

Iron-containing zeolites have a wide range of applications in petrochemical, environmental protection, fine chemical, and other catalytic processes, including ammonia-assisted selective catalytic reduction (SCR) of nitric oxide (NO) and nitrogen dioxide (NO_2), due to their microporous structure and the redox chemistry conferred by the inclusion of Fe species [1]. The nature of the incorporated Fe is critical for the catalytic properties; both the synthesis procedures and conditions and the zeolite's inherent characteristics—such as porosity and acidity—determine the state of the Fe species in the zeolite, which has a substantial influence on the material's redox properties, acidity, and stability [2–7]. Previous studies have extensively explored the behaviour of extra-framework Fe cations in zeolites, but the rôle of framework Fe species in the NH_3-SCR reaction is less well understood [3,8].

Fe-beta has emerged as one of the most robust Fe-zeolites for NH_3–SCR [9,10], maintaining its activity, and nitrogen selectivity, even after hydrothermal ageing at 750 °C [11]. BEA features 12-MR channels with diameters of 0.76 × 0.64 nm and 0.55 × 0.55 nm, ensuring good accessibility of acid sites, high thermal stability, and strong acidity making it an excellent catalyst and sorbent for a wide range of industrial processes, including NO_x reduction [12,13]. When compared to SSZ-13 and SAPO-34 zeolites, Beta zeolites stand out due to their distinctive three-dimensional twelve-element annulus structure [14]. In addition,

Abbreviations: SCR, Selective catalytic reduction; QM/MM, Quantum mechanical/molecular mechanical; DFT, Density functional theory; CHA, Chabazite; DRIFTS, Diffuse reflectance Fourier transform spectroscopy; FTIR, Fourier transform infrared; PXRD, Powder X-ray Diffraction; EDX, Energy dispersive X-ray; XANES, X-ray Absorption Near Edge Structure.

* Corresponding author.
E-mail addresses: jamal.nasir.18@ucl.ac.uk (J. Abdul Nasir), a.sokol@ucl.ac.uk (A.A. Sokol), c.r.a.catlow@ucl.ac.uk (C.R.A. Catlow).

https://doi.org/10.1016/j.jcat.2024.115696
Received 11 June 2024; Received in revised form 3 August 2024; Accepted 6 August 2024
Available online 10 August 2024

Rahkamaa-Tolonen *et al.* [15] and He *et al.* [11] have demonstrated that Beta zeolites exhibit superior thermal stability compared to Fe-ZSM-5 catalysts which suggests that Fe-BEA can offer advantages in terms of maintaining catalytic activity under high-temperature conditions, such as those encountered during exhaust system regeneration. Song *et al.* [16] studied Al-free Fe-beta as a robust catalyst for selective reduction of nitric oxide by ammonia prepared *via* post-synthesis metalation; it exhibited superior durability for NH_3-SCR of NOx, maintaining over 90 % conversion at 673 K for over 400 h. They attributed its remarkable durability and catalytic performance to the absence of framework aluminum and the stabilisation of active iron species by the zeolite structure.

It is evident from experiment that the NH_3-SCR reaction occurs on several Fe-sites with distinct mechanisms, hence leading to different turnover frequencies [17]. It was suggested that under low loading, the majority of Fe ions are present as a monomer [18] in extra-framework sites, while at higher loading oligomers of Fe are formed; Liu *et al.* reviewed different active sites of Fe including monomeric, dimeric, and oligomeric species [19]. Sazama *et al.* [20] demonstrated that Fe^{3+}-oxo species with low nuclearity, including isolated Fe monomers, are highly active in NH_3-SCR. Dahl *et al.* [18] proposed that iron monomers in Fe-beta were the active species in NH_3-SCR, although the activity of these monomers varied. Kröcher *et al.* [17] suggested that all iron species are active in NH_3-SCR catalysed by Fe-ZSM-5, with their specific activity depending on the reaction temperature. According to their findings, monomeric species were responsible for deNOx activity up to 573 K, while dimeric and oligomeric species, as well as Fe_2O_3 particles, contributed more significantly to the activity at higher temperatures. Furthermore, Lobree *et al.* [21] found a linear correlation between Fe uptake and H^+ loss up to a Fe/Al ratio of 0.56, suggesting that Fe primarily resides as an isolated species $[Fe(OH)_2]^+$. A similar one-to-one Fe^{3+}/H^+ exchange ratio has been reported on an SSZ-13 zeolite up to a Fe/Al ratio of 0.18, further supporting the prevalence of isolated Fe species at low Fe loadings [22]. Gao *et al.* [23] performed experimental analyses using UV–Vis, EPR, and Mössbauer spectroscopies, along with temperature-programmed reduction and desorption techniques, to analyse the Fe sites in SSZ-13. At low temperatures, the primary Fe species identified were extra-framework Fe(III) species, particularly $[Fe^{3+}(OH^-)_2]^+$ (monomeric). The data suggest that isolated Fe^{3+} ions, such as $[Fe^{3+}(OH^-)_2]^+$, are the active sites for low-temperature standard SCR. Fe ions (Fe^{2+} and Fe^{3+} ions) can be incorporated into the framework of high silica zeolites; subsequent high-temperature treatment of these ferrisilicates leads to the ejection of Fe from the framework and can be considered another approach for the generation of extra-framework species [24]. Furthermore, the stability of mononuclear iron species in the SSZ-13 zeolite with isolated Al has been investigated by Li *et al.* [25]. Their calculations showed that in the phase diagram for Fe species in the presence of H_2O, $[Fe^{3+}(OH^-)_2]^+$ is the most stable species at temperatures below 600 °C. Consequently, $[Fe^{3+}(OH^-)_2]^+$ was used as the initial structure for the active iron species in their study.

Another assumption regarding Fe-exchanged zeolites is that extra-framework Fe^{3+} is only coordinated to oxygen and is unstable in high silica zeolites due to the lack of negative charge within the zeolite lattice to counterbalance the trivalent ions [24]. However, there is experimental evidence that trivalent ions can be present in the framework owing to their similar charge and size as Al [24,26–28]. Thus, Fe^{3+} can be incorporated into high silica zeolites as a framework cation, although steaming of ferrisilicates—analogous to the dealumination of aluminosilicates—induces the removal of Fe from the framework introducing it into the extra-framework sites [24].

Experimental studies indeed reveal that the distribution of framework cations such as Al in zeolites often deviates from simplistic energy-based rules. While Lowenstein's rule regarding the absence of direct Al-O-Al linkages in the framework is generally observed, deviations from this rule are noted in synthetic zeolites [29,30]. We have reported the energetics of small Si-Al clusters and rings to understand the origin of Lowenstein's rule in zeolitic solids [31]. Using *ab initio* and molecular mechanics, we found that Si-O-Al bridge formation is energetically favourable over Al-O-Al bridges. Condensation reactions favour Lowensteinian configurations, particularly those with one Al species in the ring. Hydration effects also support the energetically unfavourable nature of non-Lowensteinian structures. These findings suggest that Lowenstein's rule has a kinetic basis, influenced by the energetics of small clusters formed during zeolite synthesis. However, experimental evidence provides instances where Al^{3+} substituents are found in close proximity rather than in a dispersed distribution, challenging the conventional understanding [32]. Fletcher *et al.* [45] predict deviations from Lowenstein's rule in specific forms of zeolites, suggesting potential new catalytic routes and materials. Additionally, studies employing advanced techniques such as atomic-scale analysis and microscopy reveal a non-random distribution of Al within highly crystalline zeolites [33]. This non-random distribution is further accentuated upon steaming, leading to pronounced clustering near diffusion barriers, which facilitate the transportation of Al towards the outer surface of zeolites [33]. Furthermore, observations during crystallisation indicate a steady transition of Al towards the crystal surface, sometimes accompanied by Si enrichment [34,35].

The reduction of metal ions during the reaction has a major impact on the coordination of the metal to the zeolite framework. At high temperatures and under an inert atmosphere, TMI-Zeolites (Co^{3+}, Fe^{3+}, Cu^{2+}) can undergo auto-reduction [36–38]. The auto reduction of Fe^{3+} to Fe^{2+} under He treatment has been characterised by *in situ* XAS [39,40]. The reduction of Fe^{3+} to Fe^{2+} is attributed to the desorption and dehydration of $Fe^{3+}(OH)_2$ to liberate O_2 and form two $Fe^{2+}(OH)$ species [21]. The identification and the chemistry of the Fe ions in an aqueous solution are, of course, well defined from the existence of various mono-, di-, and polymeric complexes bearing different species including oxygen, water molecules, and OH groups (depending on the reaction media, especially pH) [41,42]. Berlier *et al.*[43] examined Fe-silicalite and observed that the thermal activation causes framework Fe^{3+} species to undergo reduction to Fe^{2+}. The characterisation of such trivalent ions, especially Fe^{3+}, is challenging. Fe^{3+} is present only in acidic solutions (pH<3), where proton exchange can easily occur. These considerations may be relevant to the speciation of Fe in zeolites.

Recently, Yue *et al.* reported [44] a Cu-Fe combined system (Fe-Cu-SSZ-13), which is prepared using a 4-hour high temperature (600 °C) one-pot synthesis with activated diatomite as a silicon and iron source and a copper–amine complex as a structure-directing agent as well as a copper source. The Fe-Cu-SSZ-13 catalyst obtained exhibits excellent activity in NH_3-SCR with a wide reaction temperature window (200 – 500 °C) and good stability. Although, the combination of isolated Cu^{2+} and framework Fe^{3+} ions contributes to the improved performance of Fe-Cu-SSZ-13, the high copper loading may lead to the formation of CuO_x and deactivate the catalyst. Moreover, Song *et al.*[16] studied Al-free Fe-beta as a robust catalyst for selective reduction of nitric oxide by ammonia, prepared *via* post-synthesis metallation, which exhibited superior durability for NH_3-SCR of NO_x, and maintained over 90% conversion at 673 K for over 400 h. They attributed its remarkable durability and catalytic performance to the absence of framework aluminium and the stabilisation of active iron species by the zeolite structure. The rôle of framework-Fe^{3+} or extra-framework-Fe^{3+} is still unclear, as some studies suggest that the Fe^{3+} in the framework may not contribute to the SCR reaction and its removal from the framework under high-temperature hydrothermal ageing could lead to framework collapse [45].

Following an earlier detailed study of NH_3-SCR in the Cu-exchanged zeolite chabazite [46], here, we have investigated the NH_3-SCR reaction at several active sites of the Fe-BEA system with Fe species at both framework and extra-framework cationic sites. Density functional theory (DFT) within the quantum mechanical/molecular mechanical (QM/MM) methodology (Fig. 1) is employed to elucidate reaction mechanisms in Fe-BEA. Our study provides new insight into the NH_3-SCR

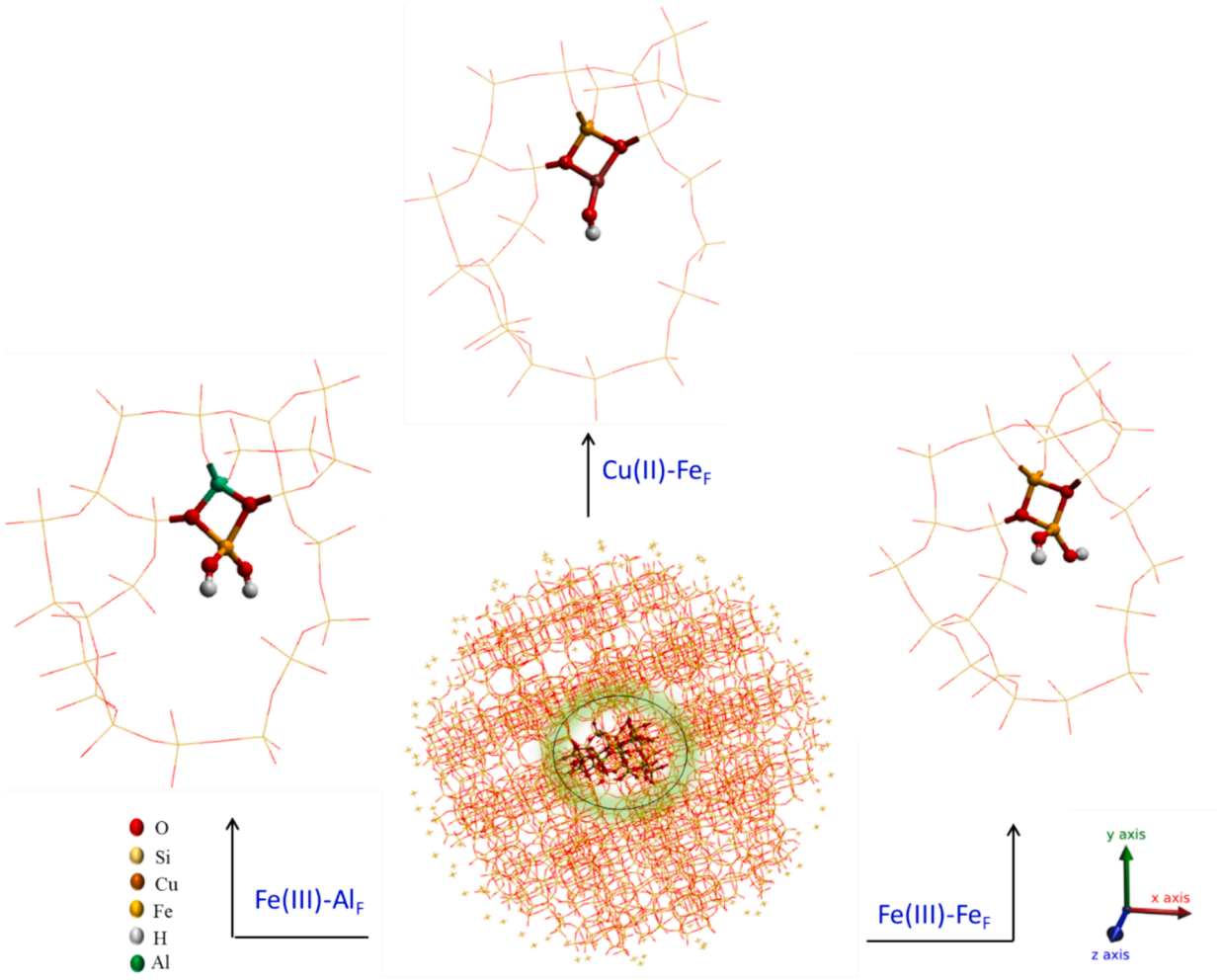

Fig. 1. The QM/MM embedding setup: the BEA cluster (centre) with a quantum mechanical region of Fe(III)-Fe$_F$-BEA, Fe-Al$_F$-BEA, and Cu-Fe$_F$-BEA. The outermost region includes point charges to ensure the Madelung potential in the centre of the cluster is accurately reproduced. **Atom colour codes**: Fe (yellow), Al (green), Cu (brown), O (red), Si (yellow), and H (white). (For interpretation of the references to colour in this figure legend, the reader is referred to the web version of this article.)

reaction by understanding the chemistry of the Fe-BEA, especially the rôle of Fe species in the key steps of the NH_3-SCR of NO_x reaction.

2. Result and discussions

We used the hybrid QM/MM techniques available in the ChemShell software package [47–49], to perform QM/MM calculations, using DFT for the quantum mechanical (QM) region, employing a general-purpose thermochemical B97-2 [50] exchange and correlation functional. However, for specific studies such as the framework Fe reduction investigation, we explored two further popular "ab-initio" functionals, PBE [51] and PBE0 [52], to assess their ability to yield results closely aligned with experimental observations. We partitioned the QM region into two segments and employed a dual basis set strategy: ~25 atoms are in the innermost QM1 region, including the intermediates which are treated with the triple-ζ basis set def2-TZVP [53] while the outer QM2 region (consisting of 64 atoms), is treated with a split valence with polarisation def2-SVP [53] basis set (see supplementary materials). QM cluster calculations were conducted using the GAMESS-UK [54] and NWChem [48] computational packages, whereas molecular mechanics (MM) simulations were performed employing the DL_POLY [55] and GULP software [56] using the Hill-Sauer Molecular Mechanical force-field [57] with charges modified following the approach by Sherwood *et al.* [58]. Geometry optimisation of the QM/MM models was carried out using the DL-FIND library [59]. For the optimisation procedures, we employed a convergence criteria where the energy change between consecutive steps was less than 1.0×10^{-6} eV, and the maximum force on each atom was below 1.0×10^{-3} eV/Å. We have investigated several candidate catalytic sites for Fe species both in framework and extra-framework locations. Our study has two main components: first, we examine the Fe-Al$_F$-BEA system, where aluminium (Al) serves as a framework cation and Fe as an extra-framework charge-balancing species. Subsequently, we modify the system by substituting the framework Al with Fe. We then introduce extra-framework cations, specifically Fe and Cu cations as illustrated in Fig. 1, which allows us to investigate the adsorption and reaction energies of reactant and product species on three different active sites.

We performed DFT calculations using the B97-2 [50] functional to determine the most favourable location for Fe in BEA zeolites and found that extra-framework Fe ions are more stable in 12MR (facing the 5-MR) compared to 5MR and 6MR by an average of 0.25 eV (24.12 kJ/mol), which is also in good agreement with previous reports suggesting that the 12MR in BEA is a suitable site for an extra-framework cation [12,13,60] (Fig. 2). In addition, Corma and co-worker [61] emphasise that zeolite nucleation is primarily governed by local interactions, with thermodynamic considerations only becoming significant when activation energies are low enough to allow for competitive reactions, which suggests that during the early stages of zeolite formation, kinetic

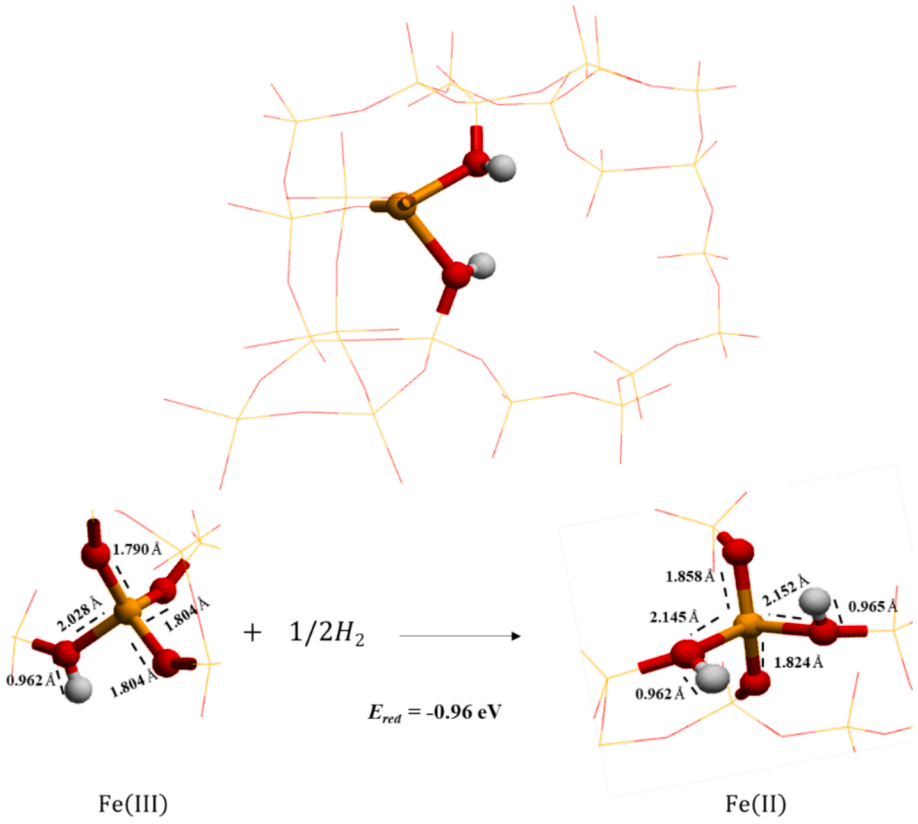

Fig. 2. Fe incorporation in BEA zeolite framework. The top panel shows Fe(II) species surrounded by the atoms included in the QM region and the bottom panel illustrates the reduction reaction of Fe(III) to Fe(II). **Atom colour codes**: Fe – yellow, O – red, and H – white. The SiO_2 framework is represented with a wire motif. (For interpretation of the references to colour in this figure legend, the reader is referred to the web version of this article.)

trapping of heteroatoms could indeed occur, influencing the distribution of heteroatoms within the framework. Furthermore, the role of organic structure-directing agents (OSDAs), as demonstrated by Navrotsky *et al.* [62], underscores the importance of kinetic factors in promoting different zeolite framework types. Hallaert *et al.* [63] investigated the nature and stability of α-Fe, and explored the binding of Fe(II) at cation exchange sites of 6MR in ZSM-5, zeolite beta, and ferrierite using DFT and multireference *ab initio* methods (CASSCF/CASPT2) and the results they obtained are in good agreement with the experimental DR-UV–Vis spectra reported by Snyder *et al.* [64]. Furthermore, Li *et al.* [65] employed *ab initio* thermodynamic techniques to assess the stability of various Fe species within ZSM-5 with Si/Al ratio of 47, and concluded that mononuclear Fe site-local $(FeO)^+$ is unaffected by the local environment, whereas binuclear sites usually occupy the larger 8-MR γ site in the sinusoidal channel. Our study focused on the framework Fe reduction process, in which framework Fe(III) is reduced to Fe(II). To study the reduction potential of framework Fe^{3+} species in the BEA zeolite (Fig. 2), we used, as noted, three DFT functionals PBE [51], PBE0 [52], B97-2 [50], and a def2-TZVP [53] basis set. All other active site components—any additional Si atoms that are first neighbours to the active site and all related linking oxygen atoms—are included in the QM zone that surrounds this central atom. Even though larger clusters are only required for larger molecules interacting with the whole channel, and may not be essential for such straightforward chemisorption processes, nevertheless, we retain the large QM region (containing 89 core atoms, not counting terminal link H atoms) in this study as discussed in the QM/MM methodology section provided with the supplementary materials. To describe the reduced Fe^{2+} state, we protonated an O atom adjacent to the central Fe species. The reduction potential energy is then defined as.

$$E^{\mathrm{red}}(\mathrm{Fe}^{3+/2+}) = E^{\mathrm{tot}}(\mathrm{Fe}^{2+}-\mathrm{BEA}) - \left[E^{\mathrm{tot}}(\mathrm{Fe}^{3+}-\mathrm{BEA}) + \tfrac{1}{2}E^{\mathrm{tot}}(\mathrm{H}_2)\right], \quad (1)$$

where $E^{\mathrm{tot}}(\mathrm{H}_2)$ is the energy of the gas-phase hydrogen dimer.

Experimental voltammetry performed by Pérez-Ramrez *et al.* [66], produced very complex reduction potential spectra ranging from –0.75 V (corresponding to −72.36 kJ/mol per electron) (C_7) to +0.65 V (C_1). The standard electrode reduction potential for $Fe^{3+}/^{2+}_{red}$ (E^o at 298 K/25 °C, 101 kPa/1 atm) is –0.771 V (i.e. −74.39 kJ/mol per electron) [67]. We thus observe a lowering of the potential on Fe accommodated by the siliceous framework which might be attributed to the significantly lower framework polarisability compared to water. In the case of zeolites, the result obtained for the framework $Fe^{3+}/^{2+}_{red}$ reduction potential in ZSM-5 by Berger *et al.* [68] employing a hybrid QM/MM technique with a numeric atomic basis set shows a negative value of –0.18 eV (−17.36 kJ/mol) using a PBE functional. Our computed value of –0.36 eV (−34.73 kJ/mol) for $Fe^{3+}/^{2+}_{red}$ for the same system (ZSM-5) using a PBE functional and triple-ζ basis set def2-TZVP [69] is lower than the value calculated by Berger *et al.* [68] which might be due to a more accurate larger QM and extensive active MM cluster employed here. Using the same computational set-up parameters, we obtained even lower values of –0.53 eV (–51.14 kJ/mol) for the BEA and –0.45 eV (–43.42 kJ/mol) for CHA zeolite systems. We then calculated the reduction energies of $Fe^{3+}/^{2+}_{red}$ in BEA using the hybrid DFT functionals PBE0 and B97-2, and obtained even lower values of –0.95 eV (–91.66 kJ/mol) and –0.96 eV (–92.62 kJ/mol), respectively. Furthermore, we performed a similar study on zeolites CHA and ZSM-5 using B97-2 and found values of –0.78 eV (–75.26 kJ/mol) and –0.62 eV (–59.82 kJ/mol), respectively. The value –0.62 eV (–59.82 kJ/mol) obtained for Fe^{3+}:V_{red} ($Fe^{3+}/^{2+}_{red}$) ZSM-5 is quite close to the experimental value (–0.7 V *vs.* SCE) [70]. The larger negative reduction potential energy observed in BEA zeolite (–0.96 eV)

(–92.62 kJ/mol) compared with ZSM-5 (–0.62 eV) (–59.82 kJ/mol) and CHA (–0.78 eV) (–75.26 kJ/mol) suggests a higher propensity for electron transfer and redox activity in the BEA system (see Table 1).

The average distances obtained in our optimised geometry for Fe(II)−O are 2.1 Å and 1.8 Å, and for Fe(III)−O are 2.02 Å, 1.8 Å and 1.79 Å. Using EXAFS, Bordiga *et al.* [27] studied Fe^{3+} as a framework cation in silicalite and demonstrated that when the counterion is a proton (Brønsted site), the tetrahedral symmetry of Fe^{3+} is significantly distorted showing long Fe−O bonds at 2.10 Å, and shorter bonds at 1.865 Å.

Next, we study the adsorption properties of three different candidate active sites (namely Fe-Al_F-BEA, Cu-Fe_F-BEA, and Fe-Fe_F-BEA) to understand their interactions with key small molecules (O_2, NH_3, H_2O, NO, and N_2); computational details are in the supplementary materials. In the case of the Fe-Al_F-BEA system, the binding of O_2, NH_3, and H_2O to the Fe(II) and Fe(III) of the Fe-BEA site is, as expected, calculated to be exothermic; in contrast, NO showed only weak interaction with both Fe (II) and Fe(III) (Fig. S1). Our results show that Fe(II) reacts exothermically with NO, consistent with experimental findings [71], although, NO adsorption on both Fe(III) and Cu(II) is found to be weak, as also indicated by TPD data, which shows negligible NO adsorption on both Fe- and Cu-zeolite catalysts [72]. In Cu-Fe_F-BEA, NH_3 strongly binds to exposed Cu(I) and Cu(II) sites. NO, on the other hand, is found to interact strongly with Cu(I) sites while weakly with Cu(II). Similarly, O_2 binds strongly to Cu(I) sites but unfavourably to Cu(II) sites (Fig. S2). After examining the properties of the Fe-Al_F-BEA and Cu-Fe_F-BEA sites, we then studied the Fe-Fe_F-BEA system, which is of particular interest (Fig. S3). NH_3 binds exothermically to Fe(II) and Fe(III) sites, while NO strongly adsorbs to Fe(II) sites but weakly to Fe(III) sites. We obtain similar results for O_2, which binds strongly to Fe(II) sites and weakly to Fe(III) sites suggesting the key rôle of O_2 in the reoxidation of Fe and Cu active sites.

The interaction of NH_3 with active sites is investigated in more detail (Fig. 3): we study the binding of NH_3 in the following order: first, the interaction with Fe Brønsted acid sites of the H-Fe_F-BEA system; second, the binding to the extra-framework cation of the framework Fe system (Cu(II)-Fe_F-BEA and Fe(III)-Fe_F-BEA); and framework Al system (Fe(III)-Al_F-BEA). Indeed, as reported in our prior work [46] and other relevant literature [73–78], Cu zeolites exhibit strong interactions with NH_3 and H_2O molecules, leading to solvation of exchanged sites, particularly under low-temperature SCR conditions. The models presented in this study aim to investigate the Fe-framework system, focusing on the fundamental interactions between single adsorbate molecules and extra-framework cations in the presence of Fe within the lattice as has been done in related studies [79,80]. Subsequent studies will build on the present work to explore solvation effects in more detail. To balance the charges, extra-framework Fe(III) is bonded to two OH species while Cu (II) to one OH. Considering first the interaction of NH_3 with Fe Brønsted acid sites (H-Fe_F-BEA system), which are often found in proximity to framework Fe cations, and are known to generate NH_4^+ ions [81–83] (Fig. 3), the formation energy of NH_4^+ ions is calculated as –1.17 eV (–112.89 kJ/mol). The experimental data on the heat of adsorption of NH_3 on zeolite Beta in the presence of framework Al (at 373 K) range from –1.03 (–99.38 kJ/mol) to –1.5 eV (–144.73 kJ/mol) for Brønsted acid sites [84,85]. The E2 (–1.14 eV) (–109.99 kJ/mol) signal usually associated with the ammonium formation has been reported by Hahn

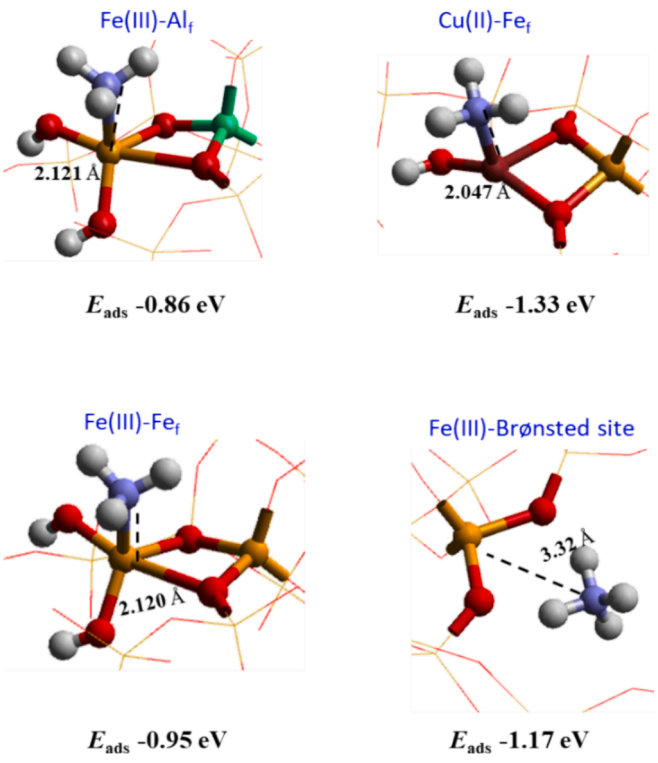

Fig. 3. The adsorption energies of NH_3 on different active sites in BEA zeolite including the Brønsted acid site. **Atom colour codes**: Fe (yellow), Al (green), Cu (brown), O (red), N (blue), and H (white). The SiO_2 framework is represented with a wire motif. (For interpretation of the references to colour in this figure legend, the reader is referred to the web version of this article.)

et al. [86] in close agreement with our calculated value. Next, we investigate the interaction of NH_3 with extra-framework cations in Cu (II)-Fe_F-BEA, Fe(III)-Fe_F-BEA, and Fe(III)-Al_F-BEA. Our calculations, summarised in Table 2 find that NH_3 exhibits a significantly stronger binding affinity with framework Fe systems: the NH_3 binding energy is –1.33 eV (–128.32 kJ/mol) to Cu(II)-Fe_F-BEA sites, compared to the reported heat of adsorption for ammonia on Cu-Beta of –1.14 eV (–109.99 kJ/mol) [87]. For comparison, our computed value of NH_3 binding with Fe(III)-Al_F-BEA active sites is –0.86 eV (–82.97 kJ/mol) while with Fe(III)-Fe_F-BEA sites it is –0.95 eV (–91.66 kJ/mol), indicating the stronger affinity of NH_3 to the framework Fe systems.

Furthermore, our QM/MM calculations show NH_3 adsorption on extra-framework Fe^{2+} results in adsorption energies of –1.50 eV (−144 kJ/mol) and −1.06 eV (−102 kJ/mol) for Fe(II)-Fe_F-BEA and Fe(II)-Al_F-BEA, respectively. The calculated value −1.06 eV (−102 kJ/mol) for Fe (II)-Al_F-BEA closely matches the value reported by Zhang *et al.* [88] on Fe-SSZ-13. Furthermore, Hahn *et al.* [89] investigated NH_3 adsorption on Fe/HBEA, and the adsorption enthalpies resulting from their kinetic model (−98.7 kJ/mol) and the differential scanning calorimetry

Table 1
Calculated $Fe^{3+/2+}$ reduction potential energies for key zeolite systems. The experimental value for $Fe^{3+}/^{2+}_{red}$ ZSM-5 reduction potential (–0.7 V *vs.* SCE) is taken from ref. [70].

Zeolite System	PBE (eV)	PBE0 (eV)	B97-2 (eV)	Experiment (V)
ZSM-5	–0.36	–	–0.62	–0.7
BEA	–0.53	–0.95	–0.96	
CHA	–0.45	–	–0.78	

Table 2
The calculated QM/MM NH_3 binding energies with various active sites of BEA zeolite.

Active site	NH_3 Binding Energy (eV)
H-Fe_F-BEA	–1.17
Fe(III)-Fe_F-BEA	–0.95
Fe(II)-Fe_F-BEA	–1.50
Cu(II)-Fe_F-BEA	–1.32
Cu(I)-Fe_F-BEA	–1.47
Fe(III)-Al_F-BEA	–0.86
Fe(II)-Al_F-BEA	–1.06
Cu(II)-Al_F-BEA	–1.16

(−117.5 kJ/mol) results [89] also agree with our computed values. In comparison, the reported average experimental heat of adsorption for ammonia on Cu-Beta and Cu-CHA [90] is approximately −1.03 eV (−100 kJ/mol). However, these experimental values should be treated with caution, as metal-exchanged zeolites still contain a significant fraction of strongly adsorbing acid sites [91,92].

2.1. Catalytic cycle

Although Fe sites in NH_3-SCR in Fe-based zeolites have been extensively studied, there is continuing debate regarding the reaction pathway. At low temperatures, the NH_3-SCR reaction typically follows the Langmuir-Hinshelwood mechanism, in which NH_3 and NO bind to the active site and produce intermediate species that subsequently break down to produce H_2O and N_2. Here, we studied the energetics of the Fe-based active sites as introduced above including Fe-Fe_F-BEA, Fe-Al_F-BEA, and Cu-Fe_F-BEA. Experimentally, switching between NH_3 + NO and NO + O_2 atmospheres enables the NH_3-SCR redox cycle to be split and the oxidation step to be isolated from the reduction step (Fig. 4) [79]. Under NH_3 + NO reductive conditions, the Fe(III)-BEA can be reduced to Fe(II)-BEA leading to the formation of nitrosamine species. The Fe(II)-BEA can then be re-oxidised as a result of the NO + O_2 oxidation process, and can generate nitrate species. The cycle in Fig. 4 including intermediates such as nitrate, nitrite and nitrosamine has been experimentally observed using DRIFTS (Diffuse Reflectance Infrared Fourier Transform Spectroscopy) experiments, as reported by Shi *et al.* [93] and Zhang *et al.* on Fe-Beta [94], and Beale *et al.* [80] and Janssens *et al.* [79] for Cu-CHA and other workers [95–100].. Experimentally, *in situ,* Fe K-edge X-ray Absorption Near Edge Structure (XANES) and DRIFTS techniques were used to monitor the $Fe^{3+} \leftrightarrow Fe^{2+}$ redox dynamics in Fe–zeolites [101–103]. We have, therefore, investigated each half of the catalytic cycle on the three active sites of the BEA zeolite computationally employing hybrid-QM/MM methodology.

2.2. Reduction of extra-framework cationic species

The introduction of NO in the presence of NH_3 under SCR reaction conditions results in the reduction of metal sites as is evident from experiment [8,104]. We employed our hybrid QM/MM calculations as described in the supplementary materials to explore the reduction of the extra-framework cationic species [Fe(III) and Cu(II)] in zeolite Beta BEA (Table 3, Fig. 5) – as shown in the following equation for Fe(III) reduction.

$$Fe(III) - (OH)_2 + NO + NH_3 \rightarrow Fe(II) - (OH) + N_2 + 2H_2O. \quad (2)$$

We studied this process for three separate active sites as described above. First, we investigate the reduction of extra-framework Fe(III) in the Fe-Al_F-BEA system. We started from the $[Fe^{3+}(OH)_2]^+$ complex which is proposed to be the most stable species below 600 °C, according to calculations made by Schneider and co-workers of the phase diagram of mononuclear Fe species at isolated Al in CHA zeolites[25]. Three spin multiplicities for Fe (III) (singlet, triplet, and quintet) were initially investigated to identify the system's most favoured spin state, with the high-spin quintet showing the lowest energy [8].

To generate NH_3-M−OH species (where M is either Fe or Cu), NH_3 molecules are first adsorbed on the cation, and the binding energy in all three cases is found to be favourable. Next, NO reacts with NH_3-M−OH species, forming NH_3-M−HONO complexes. The calculated energies indicate that NH_3-M−HONO formation is endothermic for all three sites, e.g., Fe(II)-Al_F-BEA (0.21 eV/(20.26 kJ/mol)), Fe(II)-Fe_F-BEA (0.52 eV/(50.17 kJ/mol)), and Cu(I)-Fe_F-BEA (0.11 eV/(10.61 kJ/mol)). Subsequently, NH_3-M−HONO species undergo decomposition, giving rise to an important nitrosamine (NH_2NO) intermediate which represents the reduction part of the cycle. As reported earlier, Cu^{2+}-CHA reacts with both NO and NH_3 and reduces Cu^{2+} to Cu^+ while generating N_2 and H_2O as products leading to the formation of nitrosamine species (M−N(=O)–

Table 3
The calculated QM/MM formation energies (eV) of the intermediates in the reduction part of the NH_3 SCR catalytic cycle.

Reduced catalytic sites	NH_3-M−OH	NH_3-M−HONO	(M−N(=O)–NH_2)
Fe(II)-Al_F-BEA	–0.86	0.21	–0.51
Cu(I)-Fe_F-BEA	–1.32	0.11	–0.72
Fe(II)-Fe_F-BEA	–0.95	0.52	–1.15

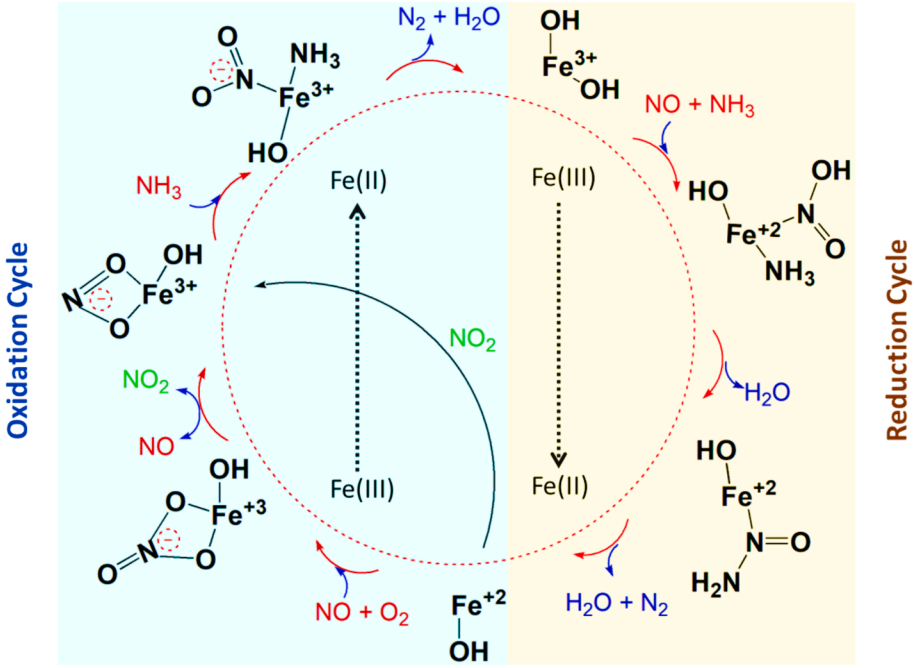

Fig. 4. Proposed catalytic cycle; yellow represents the reduction cycle and blue – the oxidation cycle. (For interpretation of the references to colour in this figure legend, the reader is referred to the web version of this article.)

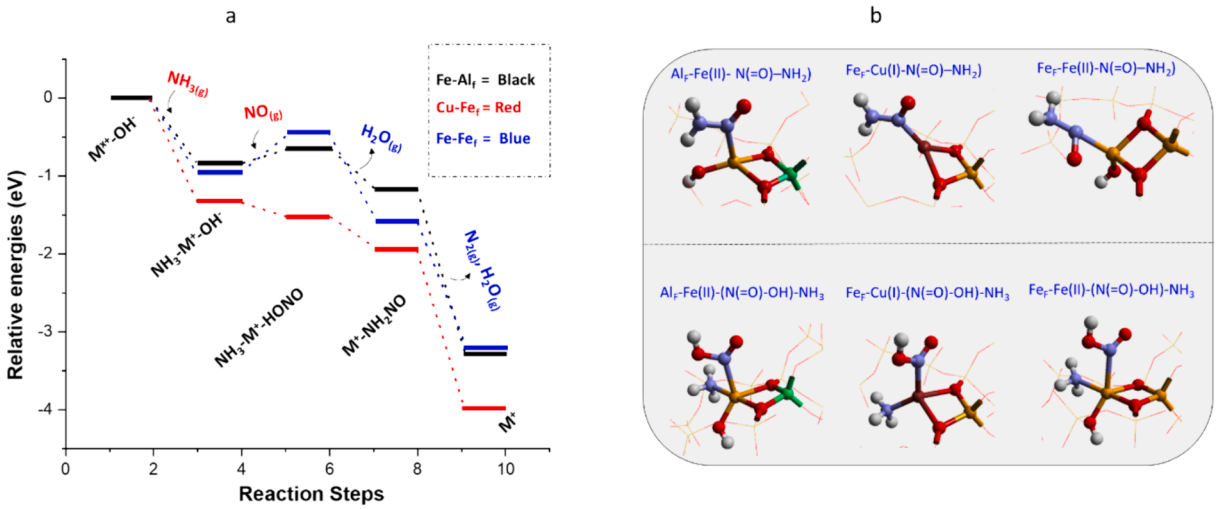

Fig. 5. (a) The reduction half cycle of the NH_3-SCR process for three active sites: Fe(III)-Al_F-BEA, Cu(II)-Fe_F-BEA, and Fe(III)-Fe_F-BEA, and (b) shows the optimized intermediates species both M−NH_2NO (upper panel) and NH_3-M−HONO (lower panel). M in the diagram represents the extra-framework metal site. **Atom colour codes**: Fe (yellow), Al (green), Cu (brown), O (red), N (blue), and H (white). The SiO_2 framework is represented with a wire motif. (For interpretation of the references to colour in this figure legend, the reader is referred to the web version of this article.)

NH_2) as is evident from both theoretical and experimental studies [46,79,80,105,106]. The computed formation energies of nitrosamine species on framework Fe sites, including Fe(II)-Fe_F-BEA (–1.15 eV/–111.94 kJ/mol)) and Cu(I)-Fe_F-BEA (–0.52 eV/(–50.17 kJ/mol)), are more favourable than on Fe(II)-Al_F-BEA (–0.51 eV/(–49.20 kJ/mol)). The collective impact of framework Fe sites is generally deemed advantageous, as exemplified by configurations such as Cu(II)-Fe_F-BEA and Fe-Fe_F-BEA. Notably, the Fe-Fe_F-BEA configuration slightly deviates from this trend, exhibiting lower favorability in the antecedent step of HONO formation when compared to counterparts like Cu(I)-Fe_F-BEA. Despite its diminished efficiency in the early stage of HONO formation, it is pertinent to recognise the overall advantage conferred by Fe framework systems including Cu(II)-Fe_F-BEA and Fe-Fe_F-BEA especially in the subsequent formation of nitrosamine species.

2.3. Oxidation of extra-framework cationic species

The adsorption of NO and O_2 on Fe(II)-BEA can generate nitrite and nitrate intermediates which undergo decomposition to N_2 and H_2O; this half cycle of the NH_3-SCR is, as noted, the oxidation part described in the following equation:

$$Fe(II) - (OH) + 2NO + O_2 + NH_3 \rightarrow Fe(III) - (OH)_2 + N_2 + H_2O + NO_2 \quad (3)$$

The re-oxidation rate has been reported to limit standard SCR rates at low temperatures[8,107,108]. Recently, we have reported [46] for the Cu-CHA zeolite that the formation of nitrate species (an important intermediate in the oxidation part of the NH_3-SCR cycle) is energetically more favourable on the solvated (NH_3, H_2O) Cu sites than in the absence of solvent molecules, demonstrating the positive influence of solvent on the oxidation component of the NH_3-SCR cycle. Previous reports suggested that gaseous NO_2 reacts with the metal site to form a bidentate

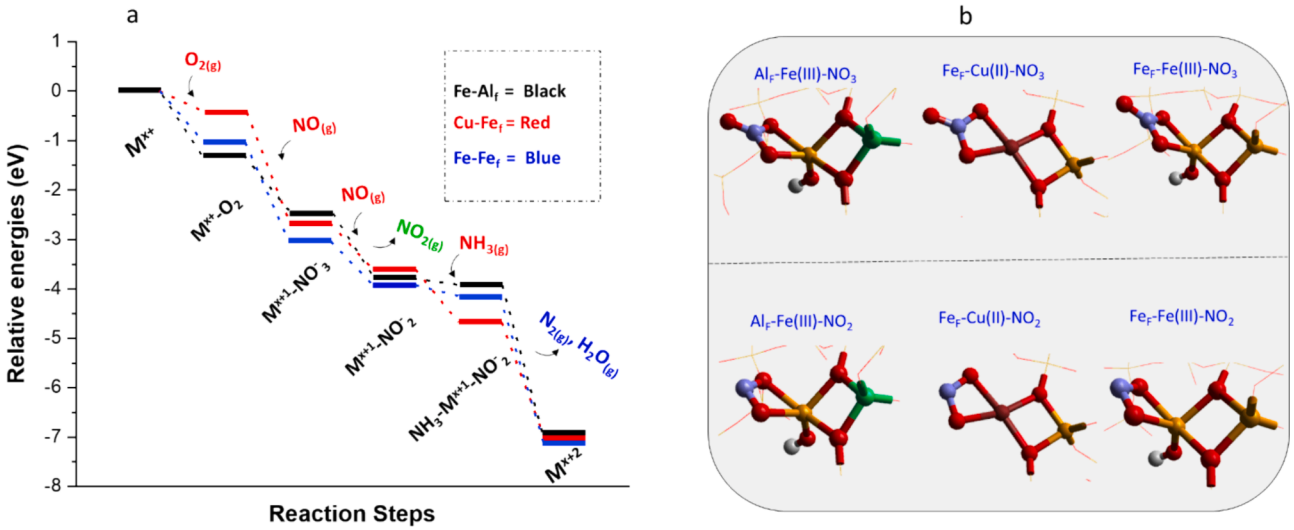

Fig. 6. Formation of nitrate: (a) the corresponding energy landscape description and (b) the schematic representation of nitrate species formation on three active sites [Fe(III)-Al_F-BEA, Cu(II)-Fe_F-BEA, and Fe(III)-Fe_F-BEA]. M in the diagram represents the extra-framework metal site. **Atom colour codes**: Fe (yellow), Al (green), Cu (brown), O (red), N (blue), and H (white). The SiO_2 framework is represented with a wire motif. (For interpretation of the references to colour in this figure legend, the reader is referred to the web version of this article.)

species—both nitrite and nitrate—a key component of the fast-selective catalytic reduction (fast-SCR) reaction [79,109,110].

To investigate the oxidation-half cycle (Fig. 6, Table 4), first, we study the activation of O_2 over Fe(II)-Al_F-BEA to generate O_2-Fe(II)-Al_F-BEA species. O_2 molecules bind to Fe(II)-Al_F-BEA species through the Fe (II) site with a binding energy of –1.26 eV (–121.57 kJ/mol). For the Fe-Fe_F-BEA system, we find the binding energy of O_2 with the Fe(II) is –1.05 eV (–101.31 kJ/mol). We also studied the adsorption of O_2 on the Cu(I) site of Cu-Fe_F-BEA system and computed a binding energy of –0.43 eV (–41.48 kJ/mol). On all three sites, the process of O_2 binding is exothermic with the most favourable sites being those with the extra-framework Fe site (Fe(II)-Fe_F-BEA, Fe-Al_F-BEA). Subsequently, we modelled the formation of the intermediate nitrate species which is formed by the interaction of NO with the activated O_2-Fe(II)-Al_F-BEA species. We calculated the formation energy of the nitrate (M−NO_3) intermediate, and the process is again investigated on the three separate active sites as shown in Table 4, and Fig. 6. As seen from the respective energy landscapes, the formation energy of nitrate species on Cu(II)-Fe_F-BEA (–1.87 eV/–180.42 kJ/mol) sites is more negative than the Fe-Al_F-BEA (–0.12 eV/–11.57 kJ/mol) and Fe-Fe_F-BEA (–0.53 eV/–51.14 kJ/mol). We find, therefore, that framework Fe systems, such as Cu(II)-Fe_F-BEA and Fe(III)-Fe_F-BEA, tend to promote the generation of nitrate species to a greater extent compared to framework Al systems like Fe-Al_F-BEA. The reaction then further proceeds through NO coordination with nitrate, forming an intermediate complex followed by decomposition of the complex to produce nitrite with the release of gaseous NO_2. Next, NH_3 reacts with the nitrite species and generates an intermediate species NH_3-M−NO_2^- with a formation energy of –0.56 eV/(–54.03 kJ/mol) and –0.29 eV (–27.98 kJ/mol) for Cu(II)-Fe_F-BEA and Fe(III)-Fe_F-BEA, respectively, in comparison to –0.15 eV (–14.47 kJ/mol) of Fe(III)-Al_F-BEA system.

2.4. Effect of ammonia solvation on Fe-Fe_F sites

Solvent molecules including water and ammonia are key components of NO_x-containing exhaust gases and their presence can lead to adsorption on transition metal sites, affecting the energetics of intermediate species. Gao *et al.* [111] highlight the significant impact of NH_3 on the NH_3-SCR process using Fe-BEA/CHA catalysts. They observed that the adsorption of NH_3 on Fe sites not only facilitates the formation of ammonium nitrate and other essential intermediates but also lowers the activation energy required for NO_x reduction, thereby improving the catalytic activity at lower temperatures. Some studies show that NH_3 helps to inhibit side reactions that could produce unwanted by-products such as N_2O [45]. Importantly, the interaction between NH_3 and Fe sites helps maintain the structural integrity of the catalyst under high-temperature conditions, which is essential for long-term industrial applications [111]. Additionally, NH_3 significantly enhances the low-temperature activity of Fe-zeolite catalysts. In our recent study [46], we also found that the formation of nitrate species on Cu-CHA zeolite is energetically more favourable on solvated active sites than on bare sites which promotes the re-oxidation part of the NH_3-SCR cycle. However, both water and ammonia inhibit the reduction part of the SCR cycle, as the formation of important intermediates like Cu-nitrosamine is less favourable on solvated sites.

We first study the reduction part of the NH_3-SCR cycle on the ammonia-solvated site (Fig. 7, Table 5). Two ammonia (N-end) molecules are coordinated to each extra-framework Fe site including both Fe(II)-Fe_F and Fe(III)-Fe_F sites. The ammonia molecules are positioned 2 Å from the Fe extra-framework centre, with the protons oriented away from adjacent oxygens and intermediate species to prevent artificial trapping in hydrogen-bonding interactions. It is important to note that hydrogen bonding with framework oxygen can significantly influence the chemistry at metal sites by affecting the binding of functionally important Fe–NH_3 units. To generate solvated NH_3-Fe-Fe_F-OH species, NH_3 molecules are adsorbed on the solvated cation, with the formation energy calculated as –0.01 eV/–0.96 kJ/mol. Next, NO reacts with NH_3-FeIII-OH species, forming NH_3-M−HONO complexes. The calculated energies indicate that the reaction energy forming NH_3-M−HONO on the solvated Fe(II)-Fe_F-BEA site is highly exothermic (–2.03 eV/–195.86 kJ/mol), while endothermic for bare Fe(II)-Fe_F-BEA (0.52 eV/50.17 kJ/mol). Subsequently, NH_3-M−HONO species decompose, yielding an important nitrosamine (NH_2NO) intermediate, which represents the reduction part of the cycle. We found that the formation of NH_2NO species is unfavourable on the solvated site (1.23 eV/118.68 kJ/mol) compared to the bare site (–1.15 eV/–110.96 kJ/mol) which also complements our previous report on Cu-CHA [46].

To investigate the oxidation-half cycle on the ammonia physisorbed Fe(II)-Fe_F sites (Fig. 8, Table 6), we first study the activation of O_2 over physisorbed Fe(II)-Fe_F-BEA to generate O_2-Fe(II)-Fe_F-BEA species and found binding energy of –1.12 eV (–108.06 kJ/mol) compared to the –1.05 eV (–101.31 kJ/mol) of the bare site. Subsequently, we study the formation of the important intermediate nitrate species which is formed by the interaction of NO with the activated O_2-Fe(II)-Fe_F-BEA species. As seen from Table 6, the formation energy of nitrate species on solvated Fe (II)-Fe_F-BEA (–1.43 eV/–137.97 kJ/mol) sites is close to the formation energy on bare Fe(II)-Fe_F-BEA site (–1.58 eV/–152.45 kJ/mol). We find, therefore, that framework Fe systems, such as Cu(II)-Fe_F-BEA and Fe (III)-Fe_F-BEA, tend to promote the generation of nitrate species to a greater extent compared to framework Al systems like Fe-Al_F-BEA. The reaction then further proceeds through NO coordination with nitrate, forming an intermediate complex followed by decomposition of the complex to produce nitrite with the release of gaseous NO_2. Next, NH_3 reacts with the nitrite species and generates an intermediate species NH_3-M−NO_2^- with the formation energy of –0.61 eV (–58.85 kJ/mol) and –0.29 eV (–27.98 kJ/mol) for solvated Fe(III)-Fe_F-BEA and bare Fe (III)-Fe_F-BEA sites, respectively.

2.5. Vibrational spectra

We performed harmonic vibrational calculations for important intermediate species. For this study, we have employed the NWChem [48] QM package to perform the vibrational calculations within the ChemShell [48,49,112] environment while for the MM environment, we use GULP (General Utility Lattice Program) [56]. To account for the offset to the experiment, we scaled the calculated harmonic values using vibrational scaling factors which are determined by comparing computational results with experimental data from a representative set of gas phase molecules; (details are in supporting information). For example, the scaling factor for N-O_{str} of nitrosamine is 0.915, and for N-N_{str} it is 0.918, and that for the N-O_{str} of nitrate is 0.943. Our main focus is to investigate nitrosamine M−N(=O)–NH_2 (N-O_{str} and N-N_{str}) and bidentate nitrate M−NO_3 (N-O_{str}) species for which infrared vibrational bands are calculated for all three active sites (Fe-Al_F-BEA, Cu-Fe_F-BEA, and Fe-Fe_F-BEA) (Table 7, Fig. 9), . In our previous report, we conducted a comprehensive vibrational study on Cu-CHA, scrutinizing intermediates that manifested during the SCR reaction [46,113]. Here, we place particular emphasis on the effects of Fe active sites in Fe-Beta, both within the framework and as extra-framework cations and their influence on the vibrational signatures of the intermediates.

First, we consider the Fe-Al_F-BEA system. The QM/MM harmonic frequencies for the N-O_{str} vibrational stretching band of the nitrosamine (M−N(=O)–NH_2) species appear at approximately 1500 cm^{-1}.

Table 4
The calculated QM/MM formation energies (eV) of the intermediates in the oxidation part of the NH_3 SCR catalytic cycle.

Oxidised catalytic site	M−O_2	M−NO_3^-	M−NO_2^-	NH_3-M−NO_2^-
Fe(III)-Al_F-BEA	–1.26	–1.38	–1.11	–0.15
Cu(II)-Fe_F-BEA	–0.43	–1.87	–0.96	–0.56
Fe(III)-Fe_F-BEA	–1.05	–1.58	–0.92	–0.29

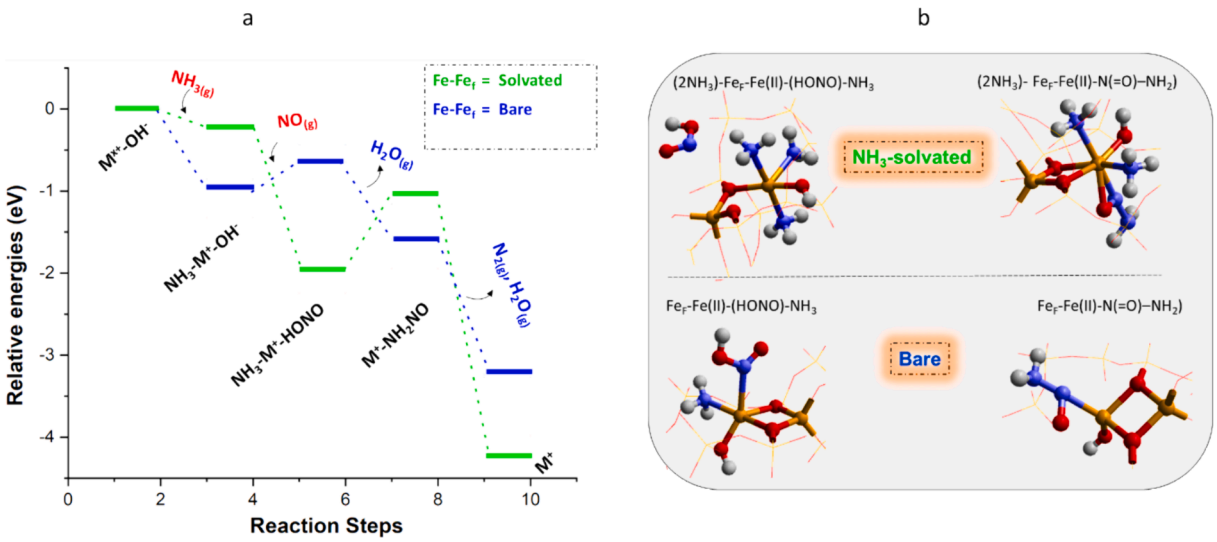

Fig. 7. (a) The potential reaction-energy landscape for the reduction part of the NH_3-SCR cycle on the solvated Fe_F-Fe BEA site; (blue) on bare-site, (green) with physisorbed ammonia, and (b) the optimized intermediates species (NH_3-M−HONO and M−NH_2NO) both solvated (upper panel) and (lower panel) without physisorbed ammonia. **Atom colour codes**: Fe (yellow), O (red), N (blue), and H (white). The SiO_2 framework is represented with a wire motif. (For interpretation of the references to colour in this figure legend, the reader is referred to the web version of this article.)

Table 5
The calculated QM/MM formation energies (eV) of the intermediates in the reduction part of the NH_3 SCR catalytic cycle on bare and activated solvated sites Fe-Fe_F active sites.

Reduced catalytic sites	NH_3-M−OH	NH_3-M−HONO	(M−N(=O)–NH_2)
Solvated-Fe(II)-Fe_F-BEA	–0.01	–2.03	1.23
Fe(II)-Fe_F-BEA	–0.95	0.52	–1.15

Experimentally, Piskorz and Urbanski [98] and Tarte [99] have found vibrational bands in the 1408 cm^{-1} – 1486 cm^{-1} range, attributing them to the N=O_{str} frequency of nonassociated dialkylnitrosamine in nonpolar solvents such as CCl_4. Kedrova *et al.* [100] have also investigated the vibrational signatures of associated nitrosamine, identifying both N=O_{str} bands in the range of 1470 cm^{-1} to 1495 cm^{-1} and N-N stretching (N-N_{str}) bands at 1055 cm^{-1} to 1060 cm^{-1}. Similarly, for N-O_{str} of nitrosamine for Cu-Fe_F-BEA, and Fe-Fe_F-BEA are calculated to be 1507 cm^{-1} and 1509 cm^{-1} respectively. Haszeldine and Jander reported a similar N=O_{str} band at 1488 cm^{-1} with strong intensity in the gas phase, consistent with their previously calculated frequency [97]. The N-N stretching frequency for the Fe-Al_F- is calculated as 1235 cm^{-1}, compared to reported experimental values in di-N-nitroso-pentamethylenetetramine (1106 cm^{-1}) and nitrosodimethylamine (1052 cm^{-1})[98]. The increase in calculated N-N_{str} frequencies may

Table 6
The calculated QM/MM formation energies (eV) of the intermediates in the oxidation part of the NH_3 SCR catalytic cycle.

Oxidised catalytic site	M−O_2	M−NO_3^-	M−NO_2^-	NH_3-M−NO_2^-
Fe(III)-Fe_F-BEA	–1.12	–1.43	–0.76	–0.61
Fe(III)-Fe_F-BEA	–1.05	–1.58	–0.92	–0.29

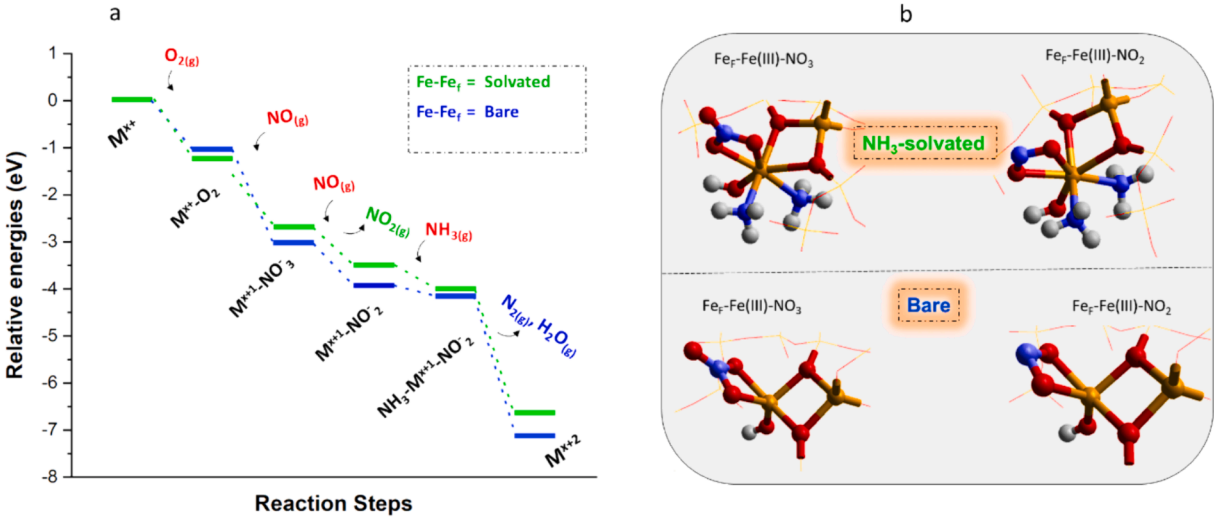

Fig. 8. (a) The potential reaction-energy landscape for the oxidation part of the NH_3-SCR cycle on the solvated Fe_F-Fe BEA site; (blue) on bare-site, (green) with physisorbed ammonia, and (b) the optimized intermediates species (M−NO_3^- and (M−NO_2^-) both solvated (upper panel) and (lower panel) without physisorbed ammonia. **Atom colour codes**: Fe (yellow), O (red), N (blue), and H (white). The SiO_2 framework is represented with a wire motif. (For interpretation of the references to colour in this figure legend, the reader is referred to the web version of this article.)

Table 7
Calculated vibrational bands of nitrate (–NO_3) and nitrosamine (N(=O)–NH_2). The assignment is based on calculated vibrational spectra and the analysis of the literature for important species shown in Fig. 4.

Vibrational mode	Calculated IR mode (cm^{-1})	Strength	Ref.
N=O stretch (nitrate)	1623 [a], 1587 [b], 1613 [c]	strong [a], strong [b], strong [c]	[95,96,116]
N=O stretch (nitrosamine)	1500 [a], 1507 [b], 1509 [c]	strong [a], strong [b], small [c]	[97–100]
N–H bend (nitrosamine)	1450 [a], 1470 [b], 1489 [c]	strong [a], medium [b], medium [c]	[117]
N–H strech (nitrosamine)	3619 [a], 3738 [b], 3616 [c]	strong [a], strong [b], small [c]	[117]
N-N stretch	1235 [a], 1192 [b], 1153 [c]	small [a], strong [b], strong [c]	[98,100]

[**a**] Fe-Al_F-BEA [**b**] Cu-Fe_F-BEA [**c**] Fe-Fe_F-BEA.

stem from a combination of N-N_{str} with N-O_{str} and N-H_{bend} modes. In Cu-Fe_F-BEA and Fe-Fe_F-BEA, N-N_{str} appears at 1192 cm^{-1} and 1153 cm^{-1}, respectively. In addition to the N=O_{str} and N-N_{str} bands for nitrosamine species, we also examined the N–H bend. The computed value for the Fe-Al-BEA is at 1450 cm^{-1}, while for the Cu-Fe_F-BEA, and Fe-Fe_F-BEA sites, it is found at 1470 cm^{-1} and 1489 cm^{-1}, respectively. Next, we focused on a bidentate nitrate (M−NO_3) species and analysed the N=O vibrational mode. Nitrate species typically exhibit four significant modes [114,115]. Our calculations revealed that the bidentate nitrate displayed the main N=O stretching frequency at 1623 cm^{-1} for Fe-Al_F-BEA which is in very good agreement with the experimental vibrational signature (1620 cm^{-1}) for the same system [116]. In comparison, the experimental N=O stretching frequency of ferric nitrate in Fe-ZSM-5 also appeared in the same region of 1622 cm^{-1} [109]. Furthermore, the calculated vibrational frequencies for the Cu-Fe_F-BEA, and Fe-Fe_F-BEA appeared at 1587 cm^{-1} and 1613 cm^{-1}, respectively.

Our hybrid-QM/MM calculations provide valuable insights into the characteristic features of nitrosamine and nitrate species across several active sites (Fe-Al_F-BEA, Cu-Fe_F-BEA, and Fe-Fe_F-BEA). The agreement between our calculated frequencies and experimental data lends credibility to our computational approach. Notably, the N-O_{str} vibrational stretching bands of nitrosamine exhibit distinct patterns in each system, allowing for the identification of unique spectroscopic fingerprints. The variation in N-N_{str} frequencies (for nitrosamine) across different active sites may be attributed to the interplay of N-N_{str} with N-O_{str} and N-H_{bend} modes. Additionally, our analysis of bidentate nitrate species reveals consistent agreement with experimental values, emphasising the accuracy of our calculations. Our computed vibrational intensity for the corresponding vibrational bands is also in good agreement with experiment. These findings contribute to a comprehensive understanding of the vibrational characteristics of these important intermediate species, paving the way for further exploration and application in catalysis.

3. Summary and conclusions

We have investigated the NH_3-SCR of NO_x reaction employing a hybrid QM/MM embedded technique over Fe-BEA catalyst. First, we have studied the reduction potential for extra-framework Fe^{3+}/Fe^{2+} in the BEA zeolite and found that the process is feasible in the presence of a Brønsted acid site. Next, we investigated the interaction of NH_3 with different active sites including the Brønsted acid of the framework Fe_F-BEA zeolite. The results show that NH_3 exhibits a stronger binding affinity with framework Fe systems, including Cu(II)-Fe_F-BEA, Fe(III)-Fe_F-BEA, and H-Fe_F-BEA compared to framework Al systems (Fe(III)-Al_F-BEA), emphasising the superior NH_3 binding strength of framework Fe sites within the zeolitic structure. Furthermore, we find that framework Fe sites, including Cu(II)-Fe_F-BEA and Fe-Fe_F-BEA, promote the formation of nitrosamines and nitrate more effectively than framework Al site (Fe-Al_F-BEA). In a separate study on solvated Fe-Fe_F active sites, it was observed that physisorbed ammonia inhibits the formation of certain intermediate species while promoting others during the reduction phase of the SCR cycle. However, the effect of physisorbed ammonia on the oxidation phase is negligible, closely following almost the same trend observed on the bare site. Through our computational analysis, we have accurately assigned key vibrational spectroscopic features associated with the important intermediates of the NH_3-SCR catalytic cycle which

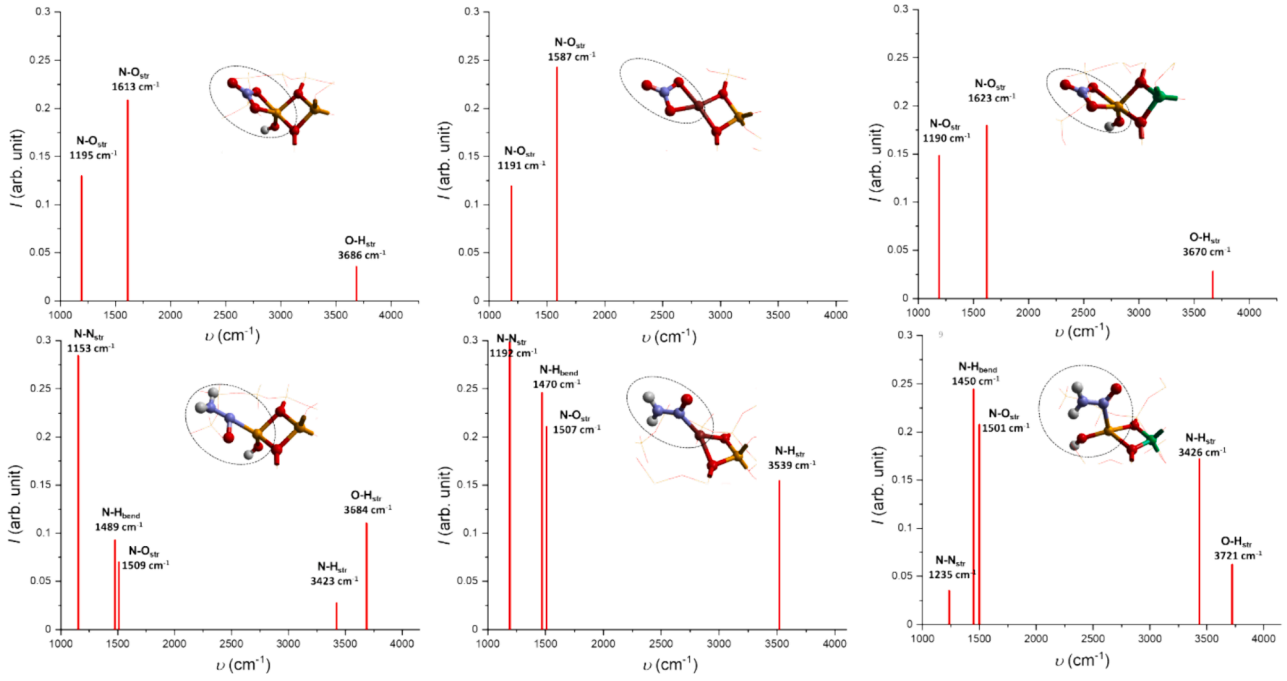

Fig. 9. Computational QM/MM IR spectra (1000–3800 cm^{-1}) capturing signatures for −bidentate-nitrate (–NO_3) above and −nitrosamine (–N(=O)–NH_2) species below. **Colour codes**: Fe (yellow), Al (green), Cu (brown), O (red), N (blue), and H (white). The SiO_2 framework is represented with a wire motif. (For interpretation of the references to colour in this figure legend, the reader is referred to the web version of this article.)

closely agree with experiment. Overall, this new study on Fe-BEA zeolite helps the understanding of how framework Fe cations influence NH_3-SCR reactions which can lead to more efficient Fe-based zeolite systems for controlling emissions.

Author contributions

The manuscript was written through contributions of all authors. All authors have given approval to the final version of the manuscript.

Funding sources

We would like to acknowledge the financial support for JAN from the Project Management Unit (PMU) Higher Education Department of KPK, Pakistan, and financial support from EPSRC.

CRediT authorship contribution statement

Jamal Abdul Nasir: Writing – original draft, Software, Methodology, Investigation, Formal analysis, Conceptualization. **Jingcheng Guan:** Writing – review & editing, Software, Methodology. **Thomas W. Keal:** Writing – review & editing, Software, Methodology. **You Lu:** Writing – review & editing, Software, Methodology. **Alexey A. Sokol:** Writing – review & editing, Supervision, Software, Methodology, Investigation. **C. Richard A. Catlow:** Writing – review & editing, Supervision.

Declaration of competing interest

The authors declare that they have no known competing financial interests or personal relationships that could have appeared to influence the work reported in this paper.

Data availability

Data will be made available on request.

Acknowledgment

The authors wish to acknowledge support from the EPSRC grants EP/R001847/1, EP/W014580/1 and EP/W014378/1, and the UK Catalysis Hub funded by EPSRC grants EP/R026939/1, and EP/R026815/1. We also wish to acknowledge the use of the ARCHER2 high-performance computing facility via the Materials Chemistry HEC Consortium (EPSRC grant EP/R029431/1 and computational support provided by CoSeC, the Computational Science Centre for Research Communities. We also thank the UCL research computing facilities. We would like to acknowledge the financial support for JAN from the Project Management Unit (PMU) Higher Education Department of KPK, Pakistan.

References

[1] J. Zhang, X. Tang, H. Yi, Q. Yu, Y. Zhang, J. Wei, Y. Yuan, Synthesis, characterization and application of Fe-zeolite: A review, Appl. Catal. A 630 (2022) 118467.
[2] T.X.H. Le, M. Drobek, M. Bechelany, J. Motuzas, A. Julbe, M. Cretin, Application of Fe-MFI zeolite catalyst in heterogeneous electro-Fenton process for water pollutants abatement, Microporous Mesoporous Mater. 278 (2019) 64–69.
[3] Q. Liu, C. Bian, S. Ming, L. Guo, S. Zhang, L. Pang, P. Liu, Z. Chen, T. Li, The opportunities and challenges of iron-zeolite as NH3-SCR catalyst in purification of vehicle exhaust, Appl. Catal. A 607 (2020) 117865.
[4] Q. Wu, H. Wang, C. Yi, Preparation of photo-Fenton heterogeneous catalyst (Fe-TS-1 zeolite) and its application in typical azo dye decoloration, J. Photochem. Photobiol. A Chem. 356 (2018) 138–149.
[5] E. Tabor, G. Sádovská, M. Bernauer, P. Sazama, J. Nováková, V. Fila, T. Kmječ, J. Kohout, K. Závěta, Z. Sobalík, Feasibility of application of iron zeolites for high-temperature decomposition of N2O under real conditions of the technology for nitric acid production, Appl Catal B 240 (2019) 358–366.
[6] R.J. Davis, New perspectives on basic zeolites as catalysts and catalyst supports, J. Catal. 216 (2003) 396–405.
[7] K. Dubkov, N. Ovanesyan, A. Shteinman, E. Starokon, G. Panov, Evolution of iron states and formation of α-sites upon activation of FeZSM-5 zeolites, J. Catal. 207 (2002) 341–352.
[8] S. Yasumura, Y. Qian, T. Kato, S. Mine, T. Toyao, Z. Maeno, K.-I. Shimizu, In Situ/Operando Spectroscopic Studies on the NH3–SCR Mechanism over Fe–Zeolites, ACS Catal. 12 (2022) 9983–9993.
[9] P. Balle, B. Geiger, S. Kureti, Selective catalytic reduction of NOx by NH3 on Fe/HBEA zeolite catalysts in oxygen-rich exhaust, Appl Catal B 85 (2009) 109–119.
[10] Z. Liu, P.J. Millington, J.E. Bailie, R.R. Rajaram, J.A. Anderson, A comparative study of the role of the support on the behaviour of iron based ammonia SCR catalysts, Microporous Mesoporous Mater. 104 (2007) 159–170.
[11] C. He, Y. Wang, Y. Cheng, C.K. Lambert, R.T. Yang, Activity, stability and hydrocarbon deactivation of Fe/Beta catalyst for SCR of NO with ammonia, Appl. Catal. A 368 (2009) 121–126.
[12] T.O. Bok, E.P. Andriako, E.E. Knyazeva, I.I. Ivanova, Engineering of zeolite BEA crystal size and morphology via seed-directed steam assisted conversion, RSC Adv. 10 (2020) 38505–38514.
[13] T. Tabata, H. Ohtsuka, L.M. Sabatino, G. Bellussi, Selective catalytic reduction of NOx by propane on Co-loaded zeolites, Microporous Mesoporous Mater. 21 (1998) 517–524.
[14] X. Guo, Z. Ding, N. Kang, L. Yang, Y. Wang, C. Zhang, Z. Li, T. Zhang, Y. Wang, Y. Wang, Ce enhanced low-temperature performance of Mn modified Cu-Beta zeolite catalyst for NH3-SCR, Fuel 361 (2024) 130694.
[15] K. Rahkamaa-Tolonen, T. Maunula, M. Lomma, M. Huuhtanen, R.L. Keiski, The effect of NO2 on the activity of fresh and aged zeolite catalysts in the NH3-SCR reaction, Catal. Today 100 (2005) 217–222.
[16] S. Song, G. Wu, W. Dai, N. Guan, L. Li, Al-free Fe-beta as a robust catalyst for selective reduction of nitric oxide by ammonia, Cat. Sci. Technol. 6 (2016) 8325–8335.
[17] S. Brandenberger, O. Kröcher, A. Tissler, R. Althoff, The determination of the activities of different iron species in Fe-ZSM-5 for SCR of NO by NH3, Appl. Catal., b. 95 (2010) 348–357.
[18] M. Høj, M.J. Beier, J.-D. Grunwaldt, S. Dahl, The role of monomeric iron during the selective catalytic reduction of NOx by NH3 over Fe-BEA zeolite catalysts, Appl Catal B 93 (2009) 166–176.
[19] F. Liu, Y. Yu, H. He, Environmentally-benign catalysts for the selective catalytic reduction of NO x from diesel engines: structure–activity relationship and reaction mechanism aspects, Chem. Commun. 50 (2014) 8445–8463.
[20] P. Sazama, B. Wichterlová, E. Tábor, P. Šťastný, N.K. Sathu, Z. Sobalík, J. Dědeček, Š. Sklenák, P. Klein, A. Vondrová, Tailoring of the structure of Fe-cationic species in Fe-ZSM-5 by distribution of Al atoms in the framework for N2O decomposition and NH3-SCR-NOx, J. Catal. 312 (2014) 123–138.
[21] L.J. Lobree, I.-C. Hwang, J.A. Reimer, A.T. Bell, Investigations of the State of Fe in H-ZSM-5, J. Catal. 186 (1999) 242–253.
[22] F. Gao, M. Kollár, R.K. Kukkadapu, N.M. Washton, Y. Wang, J. Szanyi, C. H. Peden, Fe/SSZ-13 as an NH3-SCR catalyst: A reaction kinetics and FTIR/Mössbauer spectroscopic study, Appl Catal B 164 (2015) 407–419.
[23] F. Gao, Y. Zheng, R.K. Kukkadapu, Y. Wang, E.D. Walter, B. Schwenzer, J. Szanyi, C.H. Peden, Iron loading effects in Fe/SSZ-13 NH3-SCR catalysts: nature of the Fe ions and structure–function relationships, ACS Catal. 6 (2016) 2939–2954.
[24] B. Wichterlová, Structural analysis of potential active sites in metallo-zeolites for selective catalytic reduction of NO x, An Attempt for the Structure versus Activity Relationship, Topics in Catalysis 28 (2004) 131–140.
[25] S. Li, Y. Wang, T. Wu, W.F. Schneider, First-principles analysis of site-and condition-dependent Fe speciation in SSZ-13 and implications for catalyst optimization, ACS Catal. 8 (2018) 10119–10130.
[26] S.A. Axon, K.K. Fox, S.W. Carr, J. Klinowski, EXAFS studies of iron-substituted zeolite ZSM-5, Chem. Phys. Lett. 189 (1992) 1–6.
[27] S. Bordiga, R. Buzzoni, F. Geobaldo, C. Lamberti, E. Giamello, A. Zecchina, G. Leofanti, G. Petrini, G. Tozzola, G. Vlaic, Structure and reactivity of framework and extraframework iron in Fe-silicalite as investigated by spectroscopic and physicochemical methods, J. Catal. 158 (1996) 486–501.
[28] J.A. van Bokhoven, C. Lamberti, Structure of aluminum, iron, and other heteroatoms in zeolites by X-ray absorption spectroscopy, Coord. Chem. Rev. 277 (2014) 275–290.
[29] T. Takaishi, M. Kato, K. Itabashi, Stability of the Al-O-Si-O-Al linkage in a zeolitic framework, J. Phys. Chem. 98 (1994) 5742–5743.
[30] M. Sato, K. Maeda, K. Hirasawa, Si,, Al Distribution in Zeolite Frameworks with Special Reference To Dempseys Rule, in, Studies in Surface Science and Catalysis, Elsevier (1994) 589–596.
[31] C. Catlow, A. George, C. Freeman, Ab initio and molecular-mechanics studies of aluminosilicate fragments, and the origin of Lowenstein's rule, Chem. Commun. (1996) 1311–1312.
[32] J. Dědeček, Z. Sobalík, B. Wichterlová, Siting and distribution of framework aluminium atoms in silicon-rich zeolites and impact on catalysis, Catal. Rev. 54 (2012) 135–223.
[33] D.E. Perea, I. Arslan, J. Liu, Z. Ristanović, L. Kovarik, B.W. Arey, J.A. Lercher, S. R. Bare, B.M. Weckhuysen, Determining the location and nearest neighbours of aluminium in zeolites with atom probe tomography, Nat. Commun. 6 (2015) 7589.
[34] T. Li, F. Krumeich, M. Chen, Z. Ma, J.A. van Bokhoven, Defining aluminum-zoning during synthesis of ZSM-5 zeolites, PCCP 22 (2020) 734–739.
[35] N. Omori, A. Candeo, S. Mosca, I. Lezcano-Gonzalez, I.K. Robinson, L. Li, A. G. Greenaway, P. Collier, A.M. Beale, Multimodal Imaging of Autofluorescent Sites Reveals Varied Chemical Speciation in SSZ-13 Crystals, Angew. Chem. Int. Ed. 60 (2021) 5125–5131.

[36] D. Chen, Y. Yan, A. Guo, V. Rizzotto, H. Lei, Z. Qiao, H. Liang, M. Jabłońska, X. Jiang, J. Jiang, Mechanistic insights into the promotion of low-temperature NH3-SCR catalysis by copper auto-reduction in Cu-zeolites, Appl Catal B 322 (2023) 122118.

[37] P.J. Smeets, J.S. Woertink, B.F. Sels, E.I. Solomon, R.A. Schoonheydt, Transition-metal ions in zeolites: coordination and activation of oxygen, Inorg. Chem. 49 (2010) 3573–3583.

[38] A.M. Beale, F. Gao, I. Lezcano-Gonzalez, C.H. Peden, J. Szanyi, Recent advances in automotive catalysis for NO x emission control by small-pore microporous materials, Chem. Soc. Rev. 44 (2015) 7371–7405.

[39] A. Zecchina, M. Rivallan, G. Berlier, C. Lamberti, G. Ricchiardi, Structure and nuclearity of active sites in Fe-zeolites: comparison with iron sites in enzymes and homogeneous catalysts, Phys. Chem. Chem. Phys. 9 (2007) 3483–3499.

[40] S. Lai, Y. She, W. Zhan, Y. Guo, Y. Guo, L. Wang, G. Lu, Performance of Fe-ZSM-5 for selective catalytic reduction of NOx with NH3: Effect of the atmosphere during the preparation of catalysts, J. Mol. Catal. A-Chem. 424 (2016) 232–240.

[41] C. Baes, R. Mesmer, T. Hydrolysis, of Cations,, Malabar, RE Krieger, Fla., 1976.

[42] P. Ratnasamy, R. Kumar, Ferrisilicate analogs of zeolites, Catal. Today 9 (1991) 329–416.

[43] G. Berlier, G. Spoto, P. Fisicaro, S. Bordiga, A. Zecchina, E. Giamello, C. Lamberti, Co-ordination and oxidation changes undergone by iron species in Fe-silicalite upon template removal, activation and interaction with N2O: an in situ X-ray absorption study, Microchem. J. 71 (2002) 101–116.

[44] Y. Yue, B. Liu, P. Qin, N. Lv, T. Wang, X. Bi, H. Zhu, P. Yuan, Z. Bai, Q. Cui, One-pot synthesis of FeCu-SSZ-13 zeolite with superior performance in selective catalytic reduction of NO by NH3 from natural aluminosilicates, Chem. Eng. J. 398 (2020) 125515.

[45] F. Gao, Fe-exchanged small-pore zeolites as ammonia selective catalytic reduction (NH3-SCR) catalysts, Catalysts 10 (2020) 1324.

[46] J. Abdul Nasir, J. Guan, T.W. Keal, A.W. Desmoutier, Y. Lu, A.M. Beale, C.R. A. Catlow, A.A. Sokol, Influence of solvent on selective catalytic reduction of nitrogen oxides with ammonia over Cu-CHA zeolite, J. Am. Chem. Soc. 145 (2022) 247–259.

[47] Y. Lu, K. Sen, C. Yong, D.S. Gunn, J.A. Purton, J. Guan, A. Desmoutier, J.A. Nasir, X. Zhang, L. Zhu, Multiscale QM/MM modelling of catalytic systems with ChemShell, PCCP 25 (2023) 21816–21835.

[48] Y. Lu, M.R. Farrow, P. Fayon, A.J. Logsdail, A.A. Sokol, C.R.A. Catlow, P. Sherwood, T.W. Keal, Open-source, python-based redevelopment of the ChemShell multiscale QM/MM environment, J. Chem. Theory Comput. 15 (2018) 1317–1328.

[49] P. Sherwood, A.H. de Vries, M.F. Guest, G. Schreckenbach, C.R.A. Catlow, S. A. French, A.A. Sokol, S.T. Bromley, W. Thiel, A.J. Turner, QUASI: A general purpose implementation of the QM/MM approach and its application to problems in catalysis, J. Mol. Struct. (Thoechem) 632 (2003) 1–28.

[50] P.J. Wilson, T.J. Bradley, D.J. Tozer, Hybrid exchange-correlation functional determined from thermochemical data and ab initio potentials, J. Chem. Phys. 115 (2001) 9233–9242.

[51] M. Ernzerhof, G.E. Scuseria, Assessment of the Perdew–Burke–Ernzerhof exchange-correlation functional, J. Chem. Phys. 110 (1999) 5029–5036.

[52] C. Adamo, V. Barone, Toward reliable density functional methods without adjustable parameters: The PBE0 model, J. Chem. Phys. 110 (1999) 6158–6170.

[53] F. Weigend, R. Ahlrichs, Balanced basis sets of split valence, triple zeta valence and quadruple zeta valence quality for H to Rn: Design and assessment of accuracy, PCCP 7 (2005) 3297–3305.

[54] M.F. Guest*, I.J. Bush, H.J. Van Dam, P. Sherwood, J.M. Thomas, J.H. Van Lenthe, R.W. Havenith, J. Kendrick,, The GAMESS-UK electronic structure package: algorithms, developments and applications, Mol. Phys. 103 (2005) 719–747.

[55] W. Smith, C. Yong, P. Rodger, DL_POLY: Application to molecular simulation, Mol. Simul. 28 (2002) 385–471.

[56] J.D. Gale, A.L. Rohl, The general utility lattice program (GULP), Mol. Simul. 29 (2003) 291–341.

[57] J.R. Hill, J. Sauer, Molecular mechanics potential for silica and zeolite catalysts based on ab initio calculations. 1. Dense and microporous silica, J. Phys. Chem. 98 (1994) 1238–1244.

[58] A. de Vries, S. Collins, S. Greatbanks, N. Burton, M. Vincent, I. Hillier, Computer simulation of zeolite structure and reactivity using embedded cluster methods, Faraday Discuss. 106 (1997) 79–92.

[59] J. Kästner, J.M. Carr, T.W. Keal, W. Thiel, A. Wander, P. Sherwood, DL-FIND: an open-source geometry optimizer for atomistic simulations, Chem. A Eur. J. 113 (2009) 11856–11865.

[60] M. Nakai, K. Miyake, R. Inoue, K. Ono, H. Al Jabri, Y. Hirota, Y. Uchida, M. Miyamoto, N. Nishiyama, Synthesis of high silica* BEA type ferrisilicate (Fe-Beta) by dry gel conversion method using dealuminated zeolites and its catalytic performance on acetone to olefins (ATO) reaction, Microporous Mesoporous Mater. 273 (2019) 189–195.

[61] G. Sastre, S. Leiva, M.J. Sabater, I. Gimenez, F. Rey, S. Valencia, A. Corma, Computational and experimental approach to the role of structure-directing agents in the synthesis of zeolites: The case of cyclohexyl alkyl pyrrolidinium salts in the synthesis of β, EU-1, ZSM-11, and ZSM-12 zeolites, J. Phys. Chem. B 107 (2003) 5432–5440.

[62] A. Navrotsky, O. Trofymluk, A.A. Levchenko, Thermochemistry of microporous and mesoporous materials, Chem. Rev. 109 (2009) 3885–3902.

[63] S.D. Hallaert, M.L. Bols, P. Vanelderen, R.A. Schoonheydt, B.F. Sels, K. Pierloot, Identification of α-Fe in high-silica zeolites on the basis of ab initio electronic structure calculations, Inorg. Chem. 56 (2017) 10681–10690.

[64] B.E. Snyder, P. Vanelderen, M.L. Bols, S.D. Hallaert, L.H. Böttger, L. Ungur, K. Pierloot, R.A. Schoonheydt, B.F. Sels, E.I. Solomon, The active site of low-temperature methane hydroxylation in iron-containing zeolites, Nature 536 (2016) 317–321.

[65] G. Li, E.A. Pidko, R.A. Van Santen, C. Li, E.J. Hensen, Stability of extraframework iron-containing complexes in ZSM-5 zeolite, J. Phys. Chem. C 117 (2013) 413–426.

[66] J. Pérez-Ramírez, G. Mul, F. Kapteijn, J. Moulijn, A. Overweg, A. Doménech, A. Ribera, I. Arends, Physicochemical characterization of isomorphously substituted FeZSM-5 during activation, J. Catal. 207 (2002) 113–126.

[67] S.G. Bratsch, Standard electrode potentials and temperature coefficients in water at 298.15 K, J. Phys. Chem. Ref. Data 18 (1989) 1–21.

[68] D. Berger, A.J. Logsdail, H. Oberhofer, M.R. Farrow, C.R.A. Catlow, P. Sherwood, A.A. Sokol, V. Blum, K. Reuter, Embedded-cluster calculations in a numeric atomic orbital density-functional theory framework, J. Chem. Phys. 141 (2014) 024105.

[69] J. Zheng, X. Xu, D.G. Truhlar, Minimally augmented Karlsruhe basis sets, Theor. Chem. Acc. 128 (2011) 295–305.

[70] Z. Bencheqroun, N.E. Sahin, O.S. Soares, M.F. Pereira, H. Zaitan, M. Nawdali, E. Rombi, A.M. Fonseca, P. Parpot, I.C. Neves, Fe (III)-exchanged zeolites as efficient electrocatalysts for Fenton-like oxidation of dyes in aqueous phase, J. Environ. Chem. Eng. 10 (2022) 107891.

[71] R. Long, R. Yang, Catalytic performance of Fe–ZSM-5 catalysts for selective catalytic reduction of nitric oxide by ammonia, J. Catal. 188 (1999) 332–339.

[72] P.S. Metkar, V. Balakotaiah, M.P. Harold, Experimental and kinetic modeling study of NO oxidation: Comparison of Fe and Cu-zeolite catalysts, Catal. Today 184 (2012) 115–128.

[73] K.A. Lomachenko, E. Borfecchia, C. Negri, G. Berlier, C. Lamberti, P. Beato, H. Falsig, S. Bordiga, The Cu-CHA deNO x catalyst in action: temperature-dependent NH3-assisted selective catalytic reduction monitored by operando XAS and XES, J. Am. Chem. Soc. 138 (2016) 12025–12028.

[74] X. Wang, L. Chen, P.N. Vennestrøm, T.V. Janssens, J. Jansson, H. Grönbeck, M. Skoglundh, Direct measurement of enthalpy and entropy changes in NH3 promoted O2 activation over Cu− CHA at low temperature, ChemCatChem 13 (2021) 2577–2582.

[75] C. Paolucci, I. Khurana, A.A. Parekh, S. Li, A.J. Shih, H. Li, J.R. Di Iorio, J. D. Albarracin-Caballero, A. Yezerets, J.T. Miller, Dynamic multinuclear sites formed by mobilized copper ions in NOx selective catalytic reduction, Science 357 (2017) 898–903.

[76] S.H. Krishna, A. Goswami, Y. Wang, C.B. Jones, D.P. Dean, J.T. Miller, W. F. Schneider, R. Gounder, Influence of framework Al density in chabazite zeolites on copper ion mobility and reactivity during NO x selective catalytic reduction with NH3, Nat. Catal. 6 (2023) 276–285.

[77] P. Chen, V. Rizzotto, A. Khetan, K. Xie, R. Moos, H. Pitsch, D. Ye, U. Simon, Mechanistic understanding of Cu-CHA catalyst as sensor for direct NH3-SCR monitoring: the role of Cu mobility, ACS Appl. Mater. Interfaces 11 (2019) 8097–8105.

[78] A. Marberger, A.W. Petrov, P. Steiger, M. Elsener, O. Kröcher, M. Nachtegaal, D. Ferri, Time-resolved copper speciation during selective catalytic reduction of NO on Cu-SSZ-13, Nat. Catal. 1 (2018) 221.

[79] T.V. Janssens, H. Falsig, L.F. Lundegaard, P.N. Vennestrøm, S.B. Rasmussen, P. G. Moses, F. Giordanino, E. Borfecchia, K.A. Lomachenko, C. Lamberti, A consistent reaction scheme for the selective catalytic reduction of nitrogen oxides with ammonia, ACS Catal. 5 (2015) 2832–2845.

[80] A.G. Greenaway, A. Marberger, A. Thetford, I. Lezcano-González, M. Agote-Arán, M. Nachtegaal, D. Ferri, O. Kröcher, C.R.A. Catlow, A.M. Beale, Detection of key transient Cu intermediates in SSZ-13 during NH 3-SCR deNO x by modulation excitation IR spectroscopy, Chem. Sci. 11 (2020) 447–455.

[81] M. Brändle, J. Sauer, Acidity differences between inorganic solids induced by their framework structure, A Combined Quantum Mechanics/molecular Mechanics Ab Initio Study on Zeolites, Journal of the American Chemical Society 120 (1998) 1556–1570.

[82] U. Eichler, M. Brändle, J. Sauer, Predicting absolute and site specific acidities for zeolite catalysts by a combined quantum mechanics/interatomic potential function approach, J. Phys. Chem. B 101 (1997) 10035–10050.

[83] J. Sauer, Acidic sites in heterogeneous catalysis: structure, properties and activity, J. Mol. Catal. 54 (1989) 312–323.

[84] K. Suzuki, T. Noda, N. Katada, M. Niwa, IRMS-TPD of ammonia: Direct and individual measurement of Brønsted acidity in zeolites and its relationship with the catalytic cracking activity, J. Catal. 250 (2007) 151–160.

[85] S.A. Skarlis, D. Berthout, A. Nicolle, C. Dujardin, P. Granger, IR spectroscopy analysis and kinetic modeling study for NH3 adsorption and desorption on H-and Fe-BEA catalysts, J. Phys. Chem. C 117 (2013) 7154–7169.

[86] C. Hahn, S. Füger, M. Endisch, A. Pacher, S. Kureti, Kinetic modelling of the adsorption and desorption of NH3 on Fe/BEA Zeolite, Z. Phys. Chem. 229 (2015) 739–757.

[87] N. Wilken, K. Kamasamudram, N.W. Currier, J. Li, A. Yezerets, L. Olsson, Heat of adsorption for NH3, NO2 and NO on Cu-Beta zeolite using microcalorimeter for NH3 SCR applications, Catal. Today 151 (2010) 237–243.

[88] R. Zhang, E. Anderst, K. Groden, J.-S. McEwen, Modeling the adsorption of NO and NH3 on Fe-SSZ-13 from first-principles: a DFT study, Ind. Eng. Chem. Res. 57 (2018) 13396–13405.

[89] C. Hahn, J. Seidel, F. Mertens, S. Kureti, Study on the kinetics of the adsorption and desorption of NH 3 on Fe/HBEA zeolite, PCCP 24 (2022) 7493–7504.

[90] L. Olsson, K. Wijayanti, K. Leistner, A. Kumar, S.Y. Joshi, K. Kamasamudram, N. W. Currier, A. Yezerets, A multi-site kinetic model for NH3-SCR over Cu/SSZ-13, Appl Catal B 174 (2015) 212–224.
[91] M. Krossner, J. Sauer, Interaction of water with Brønsted acidic sites of zeolite catalysts. Ab initio study of 1: 1 and 2: 1 surface complexes, J. Phys. Chem. 100 (1996) 6199–6211.
[92] H. Jobic, A. Tuel, M. Krossner, J. Sauer, Water in interaction with acid sites in H-ZSM-5 zeolite does not form hydroxonium ions, A Comparison between Neutron Scattering Results and Ab Initio Calculations, the Journal of Physical Chemistry 100 (1996) 19545–19550.
[93] J. Shi, Y. Zhang, Z. Zhang, Z. Fan, M. Chen, Z. Zhang, W. Shangguan, Water promotion mechanism on the NH3-SCR over Fe-BEA catalyst, Catal. Commun. 115 (2018) 59–63.
[94] Y. Zhang, P. Wang, H. Zhao, X. Lyu, L. Lei, L. Zhang, The promoting mechanism of Ce on the hydrothermal stability of Fe-Beta catalyst for NH3-SCR reaction, Microporous Mesoporous Mater. 338 (2022) 111937.
[95] S. Bordiga, C. Lamberti, F. Bonino, A. Travert, F. Thibault-Starzyk, Probing zeolites by vibrational spectroscopies, Chem. Soc. Rev. 44 (2015) 7262–7341.
[96] C. Negri, P.S. Hammershøi, T.V. Janssens, P. Beato, G. Berlier, S. Bordiga, Investigating the Low Temperature Formation of CuII-(N, O) Species on Cu-CHA Zeolites for the Selective Catalytic Reduction of NOx, Chemistry–A, European Journal 24 (2018) 12044–12053.
[97] R. Haszeldine, J. Jander, Further remarks on the spectra of nitrites and nitrosamines, J. Chem. Phys. 23 (1955) 979–980.
[98] M. Piskorz, T. Urbanski, Ultraviolet and infrared spectra of some nitrosamines, Bull. Acad. Pol. Sci., Ser. Sci. Chim 11 (1963).
[99] P. Tarte, Recherches spectroscopiques sur les composés nitrosés, Bulletin Des Sociétés Chimiques Belges 63 (1954) 525–541.
[100] T. Kedrova, R. Gafurov, E. Sogomonyan, L. Eremenko, Spectroscopic study of (nitroalkyl) nitrosamines, Bulletin of the Academy of Sciences of the USSR, Division of Chemical Science 28 (1979) 944–947.
[101] J. Shi, Y. Zhang, Y. Zhu, M. Chen, Z. Zhang, W. Shangguan, Efficient Fe-ZSM-5 catalyst with wide active temperature window for NH3 selective catalytic reduction of NO: Synergistic effect of isolated Fe3+ and Fe2O3, J. Catal. 378 (2019) 17–27.
[102] M. Agote-Arán, I. Lezcano-González, A.G. Greenaway, S. Hayama, S. Díaz-Moreno, A.B. Kroner, A.M. Beale, Operando HERFD-XANES/XES studies reveal differences in the activity of Fe-species in MFI and CHA structures for the standard selective catalytic reduction of NO with NH3, Appl. Catal. A 570 (2019) 283–291.
[103] A. Boubnov, H.W. Carvalho, D.E. Doronkin, T. Günter, E. Gallo, A.J. Atkins, C. R. Jacob, J.-D. Grunwaldt, Selective catalytic reduction of NO over Fe-ZSM-5: mechanistic insights by operando HERFD-XANES and valence-to-core X-ray emission spectroscopy, J. Am. Chem. Soc. 136 (2014) 13006–13015.
[104] C. Paolucci, A.A. Verma, S.A. Bates, V.F. Kispersky, J.T. Miller, R. Gounder, W. N. Delgass, F.H. Ribeiro, W.F. Schneider, Isolation of the copper redox steps in the standard selective catalytic reduction on Cu-SSZ-13, Angew. Chem. Int. Ed. 53 (2014) 11828–11833.
[105] Y. Mao, H.F. Wang, P. Hu, Theoretical investigation of NH3-SCR processes over zeolites: A review, Int. J. Quantum Chem 115 (2015) 618–630.
[106] R. Millan, P. Cnudde, A.E. Hoffman, C.W. Lopes, P. Concepción, V. Van Speybroeck, M. Boronat, Theoretical and Spectroscopic Evidence of the Dynamic Nature of Copper Active Sites in Cu-CHA Catalysts under Selective Catalytic Reduction (NH3–SCR–NO x) Conditions, The Journal of Physical Chemistry Letters 11 (2020) 10060–10066.
[107] F. Gao, D. Mei, Y. Wang, J. Szanyi, C.H. Peden, Selective catalytic reduction over Cu/SSZ-13: linking homo-and heterogeneous catalysis, J. Am. Chem. Soc. 139 (2017) 4935–4942.
[108] C. Paolucci, I. Khurana, A.A. Parekh, S. Li, A.J. Shih, H. Li, J.R. Di Iorio, J. D. Albarracin-Caballero, A. Yezerets, J.T. Miller, Dynamic multinuclear sites formed by mobilized copper ions in NO x selective catalytic reduction, Science 357 (2017) 898–903.
[109] X. Shi, Y. Wang, Y. Shan, Y. Yu, H. He, Investigation of the common intermediates over Fe-ZSM-5 in NH3-SCR reaction at low temperature by in situ DRIFTS, J. Environ. Sci. 94 (2020) 32–39.
[110] M. Bendrich, A. Scheuer, R. Hayes, M. Votsmeier, Unified mechanistic model for Standard SCR, Fast SCR, and NO2 SCR over a copper chabazite catalyst, Appl Catal B 222 (2018) 76–87.
[111] F. Gao, J. Szanyi, Y. Wang, B. Schwenzer, M. Kollár, C.H. Peden, Hydrothermal aging effects on Fe/SSZ-13 and Fe/Beta NH3–SCR catalysts, Top. Catal. 59 (2016) 882–886.
[112] S. Metz, J. Kästner, A.A. Sokol, T.W. Keal, P. Sherwood, C hem S hell—a modular software package for QM/MM simulations, Wiley Interdiscip. Rev.: Comput. Mol. Sci. 4 (2014) 101–110.
[113] J. Guan, Y. Lu, K. Sen, J. Abdul Nasir, A.W. Desmoutier, Q. Hou, X. Zhang, A. J. Logsdail, G. Dutta, A.M. Beale, Computational infrared and Raman spectra by hybrid QM/MM techniques: a study on molecular and catalytic material systems, Phil. Trans. R. Soc. A 381 (2023) 20220234.
[114] F. Zapata, C. García-Ruiz, The discrimination of 72 nitrate, chlorate and perchlorate salts using IR and Raman spectroscopy, Spectrochim. Acta A Mol. Biomol. Spectrosc. 189 (2018) 535–542.
[115] L. Volod'Ko, L.T. Huoah, The vibrational spectra of aqueous nitrate solutions, J. Appl. Spectrosc. 9 (1968) 1100–1104.
[116] M. Jabłońska, G.r. Delahay, K. Kruczała, A. Błachowski, K.A. Tarach, K. Brylewska, C. Petitto, K. Góra-Marek,, Standard and fast selective catalytic reduction of NO with NH3 on zeolites Fe-BEA, J. Phys. Chem. C 120 (2016) 16831–16842.
[117] B.C. Smith Organic nitrogen compounds II: primary amines Spectroscopy 34 2019 22–25-22-25.